StratoSolar Tutorial

Introduction: The goal of this document is to present a short technical introduction while conveying the message that there is a much deeper body of data, analysis, and development effort underlying and supporting this brief summary. There are four main sections: an overview, technical basics, detailed analysis and miscellaneous topics

Overview

What the system does:

- Weather independent, 24/7 concentrated solar power (CSP)
- Locations up to latitude 60
- Electricity in utility scale systems up to 1 GWe
- Cost competitive with the lowest-cost coal-fired systems

Why it comes at a reasonable cost:

For solar-power plants, almost the complete operating cost is the loan payment. The StratoSolar system has a reasonable operating cost mostly because the solar concentrator (which dominates CSP cost) has a reasonable capital cost, with a resulting reasonable loan payment. The reasons for this are:

- The concentrator is exposed to 3X the solar radiation (or more) of ground-based CSP
- It captures more than 2X ground-based CSP concentrators (no cosine losses)
- This means each square meter of mirror gathers over 6X the power of ground-based CSP
- The concentrator uses no land. No land cost, or site development cost.
- Uses very little material due to a lightweight structure.
- All materials are standard, off the shelf, and low cost
- This results in mirrors that are 2X lower cost than ground-based CSP mirrors

The overall concentrator cost advantage over ground-based CSP exceeds 15X. See the detailed analysis section below (CSP cost) for more detail on this topic.
This is the first commercially competitive alternative energy solution. By not covering huge land areas, it saves on an expensive, highly regulated, and uncertain resource that tends to delay construction and limit financing options. It also allows great flexibility in location. The competitive and highly profitable economics should lead to a business that is market financed and does not need government support or subsidy once demonstrated. It is a bonus that this energy is carbon-free, and solves energy security issues

The idea:

A solar concentrator, permanently positioned in the stratosphere at altitude 10 km to 20 km, gathers and concentrates sunlight and transmits it down a hollow light-pipe to the ground where the sunlight is absorbed, stored as heat, and converted to electricity via turbines and generators.

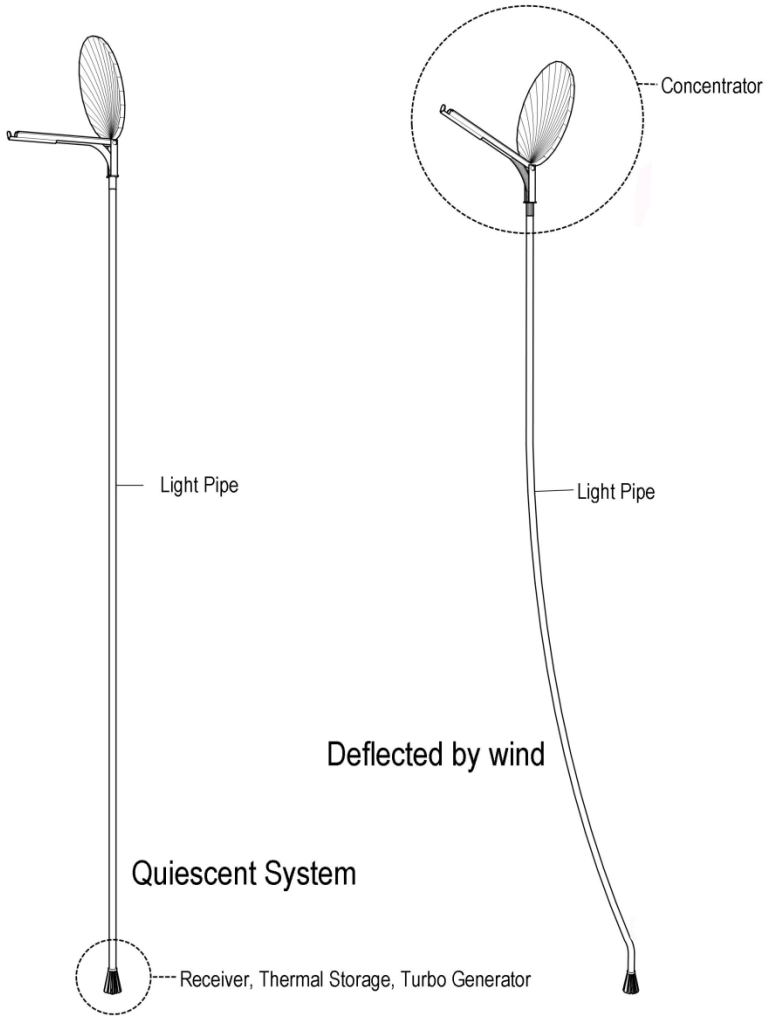

Figure 1

A StratoSolar power plant has two novel components: the solar concentrator and the light-pipe. Both are buoyant structures. The light-pipe is a hollow strong tether with a reflective inner surface. It is not a tower. Gasbags arranged as a sleeve around the exterior of the light-pipe along the top 5 km provide buoyancy. Buoyancy pre-tensions the tether and causes it to resist wind forces. Figure 1 shows two

views of the system, the first with no wind and pointing to the horizon, the second with a wind load and tracking the sun. Figure 18 and Figure 19 show graphic renderings of such a system positioned at the site of an existing power plant at Colusa in northern California at dawn on the winter solstice. The light-pipe shown is 20 km long and 160 m in diameter. The mirror is 2.3 km in diameter. Production systems will have a 30 m diameter light pipe.

The solar concentrator is a rigid truss structure supporting actively controlled mirror segments. Buoyancy is from gasbags within the truss framework. The concept exploits classical optics and modern structural engineering. Models for both the light-pipe and concentrator are subject to simulation to a high degree of accuracy, with high confidence in the results. While the structures are novel, there is no new science, and existing engineering design tools are sufficient. The wind and buoyancy forces are well-understood physics. There are detailed meteorological models and historical data to provide an accurate statistical profile of the wind and buoyancy forces on the structures. The combination of accurate structural analysis and reliable meteorological data mean that structural viability can be determined to a high confidence level before construction. Modern optical ray-tracing tools combined with the structural analysis tools accurately simulate the complete optical system. This combined with accurate models for sunlight and how it varies with location and altitude, daily and seasonally, provides an equally high confidence level for the power output.

Does it violate physics or general practicality?

No. The idea exploits two environmental facts. Firstly, the stratosphere is a permanent inversion layer in the earth's atmosphere. Inversion layers effectively isolate gas bodies. The calm stratosphere is isolated from the turbulent troposphere below. There is no weather above this layer and not much wind force. The residual wind is steady. Secondly, light from the sun is highly collimated. After concentration, a light-pipe can transmit it to the ground with little loss.

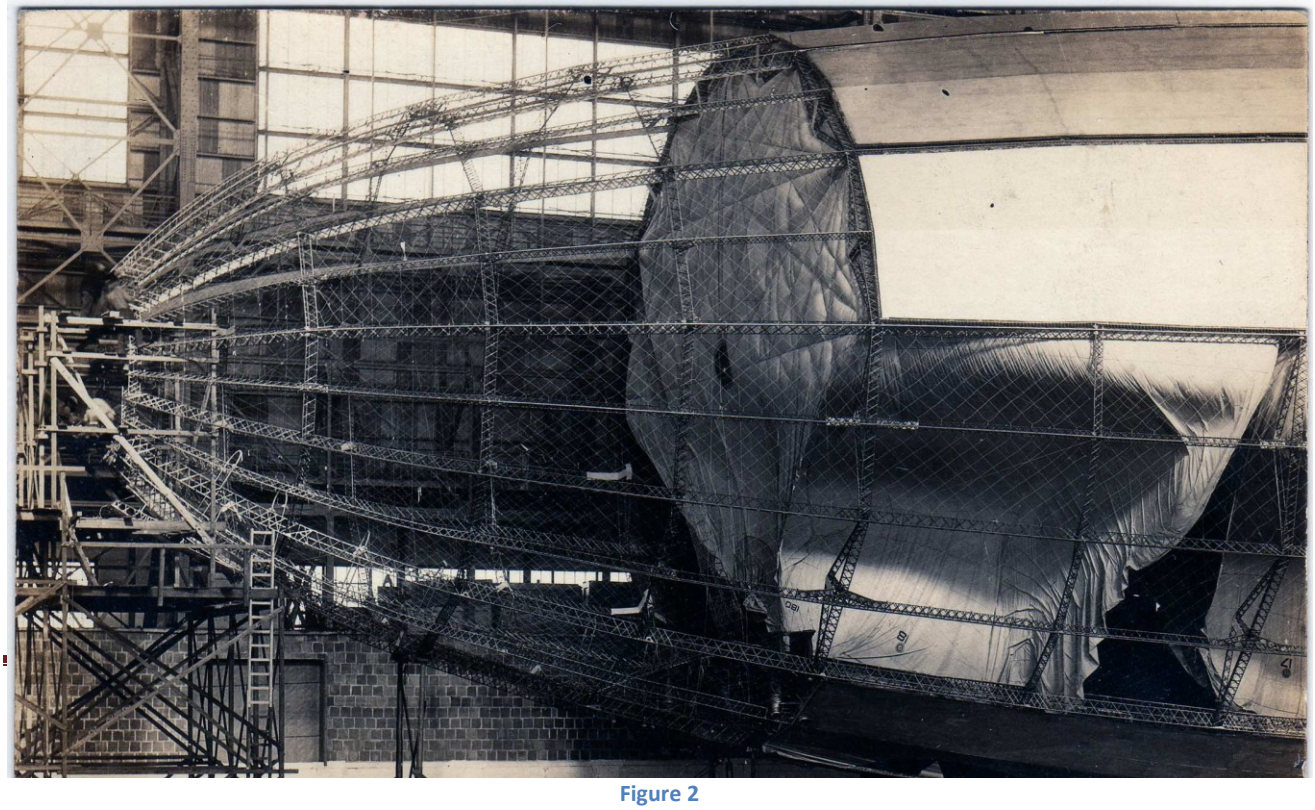

Figure 2

How far removed is it from what has been done before?

The largest rigid buoyant structures were rigid airships built in the 1930's and these displaced about 300 tonnes. This was at low altitude of less than 5000 m. However, these show all the basic technologies required in rigid structures and gasbags.

Figure 2 shows the interior structural elements of the Shenandoah. There are rigid triangular aluminum alloy struts, ropes across the struts to contain the gasbag, the partially filled gasbag, and the separate tensioned membrane exterior weatherproof skin all clearly visible. Figure 25 shows the similar internal structural elements of the Hindenburg and the Macon.

A prototype solar concentrator system would displace about 300 tonnes at 20 km and use the same structural elements but more modern materials. Utility scale systems of 10,000 to 20,000 tonnes are a significant jump in scale. Buoyant rigid systems (ships) can scale indefinitely. Other constraints, such as handling in the case of ships set the limits.

The highest tethered aerostats have been at about 8 km [(1)] TCOM (Figure 26), though science projects have proposed and investigated 12 km and higher [(2)]. Most research balloons that have flown in the stratosphere have been untethered.

Light-pipes have transmitted very large power in the MW range, but these are solid light-pipes. Hollow gas or air-filled light-pipes, for example 3M 2301, have transmitted light efficiently for illumination. These have all been relatively short, less than 50 m. However when judged by technical parameters that can scale, they have the desired properties. Power densities in lighting systems have been limited to 200 kW/m^2 by safety concerns, and aspect ratios (length/diameter) of 100:1 to 200:1 are common. A 20 km long 163 m diameter light-pipe (aspect ratio 122:1) transferring light at 200 kW/m^2 transfers about 4 GW of light power. That results in about 1 GW 24/7 electrical power after storage and conversion.

For this concept to become commercially viable what are the real problems and what technologies are available to solve them?

Both of these are long lists, and represent the engineering design and development process. This is broken down into many pieces and many sequential steps of increasing detail and complexity as a design. However, it is important to realize that the problem is still just basic structures and optics. The uncertainties nearly all stem from unfamiliarity. The data exists, the design methodologies exist and the materials are standard aluminum alloy, steel and plastics. The risk factors are the same risks faced in all large-scale structures. The balance of importance may be different but fire, lightning, ice, weathering, wind, etc. are always issues faced (and solved) by all large-scale structures.

The mirror structure does not face water-based weathering or dust and dirt, but does face increased UV, ozone and cold. Depending on altitude the light-pipe faces a variety of weather effects including rain, hail, icing and lightning strikes.

The two larger questions are about big environmental inputs, the sun and the wind. How much light is there at 20 km and how does it vary by location, time of year, and time of day? What are the dispersion and wavelength characteristics? How much wind is there through the 20 km vertical profile, and how does it vary statistically by time and location?

At this stage, we have accurate models for both wind and sunlight. These provide high confidence that the structural and optical designs are practical.

The StratoSolar concept is now at a similar stage to concentrated solar power (CSP) when it was first proposed. It's clear that it is physically possible. The questions revolve around the practicality. It took building Solar1 in Barstow to address the myriad concerns about the practicality of CSP. StratoSolar is an evolution of CSP. It is feasible based on detailed simulation. It needs to pass the practicality hurdle. Our plan is to do this incrementally and at low cost.

The first step is an 18-month R&D effort that will develop the design of a prototype system and accurately simulate its mechanical and optical behavior. The R&D phase will also develop the small-scale elements of the prototype system, such as struts, nodes, mirror segments and light pipe wall materials.

The second step is to construct a prototype system using the elements developed during step one.

Technical Basics:

Concentrator Structure:

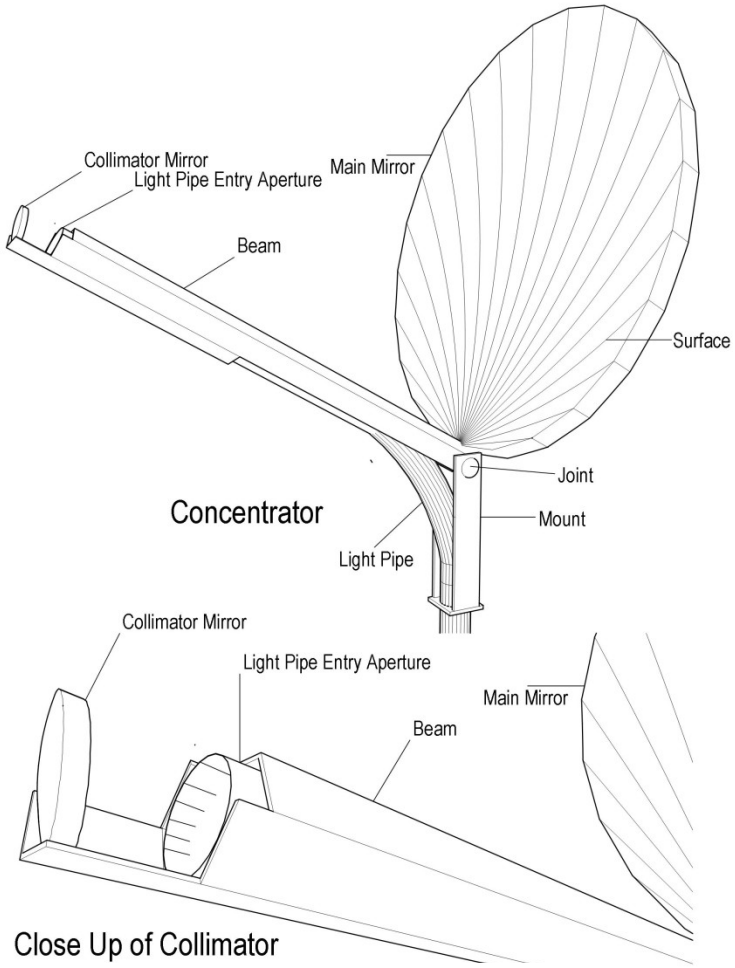

Figure 3

The mirror structure is similar to the structure of large ground-based radio telescopes and satellite receivers. For reference, the Green Bank radio telescope (Figure 20 and Figure 21) has a diameter of about 100 m and a mass of about 7,500 tonnes. The 1 GWe solar collector structure is similar to the Green Bank telescope with its dimensions scaled by approximately a factor of 20, but its mass is only approximately twice that of the Green Bank telescope.

A few simple calculations using the Archimedes principle show that making the collector a buoyant structure violates no laws of physics or practicality. Let us model the collector as a disk 2000 m in diameter and 200 m thick with the volume filled with hydrogen gasbags. The volume is then approx. 6.28e8 m^3. The density of air at 20 km is about one tenth that at sea level and 1 m^3 filled with hydrogen can lift about 0.1 kg. The disk structure can then lift about 6.28e7 kg, or 62,800 tonnes, about four times the requirement. Buoyancy becomes more effective as the volume to surface area ratio increases.

Figure 3 shows an example of a concentrator structure. The mirror shown is 2300 m in diameter. The contour lines indicate the offset parabolic curved surface. The beam holds the offset parabolic collimator mirror at the common focus. The beam also supports the light-pipe. The pivot connects the mount to the mirror/beam assembly. This allows the structure to tilt in altitude. The mount rotates in azimuth. The structure tracks the sun by controlling these two rotations.

Being a buoyant structure with the buoyancy evenly distributed throughout, the structure does not have to sustain its own weight. This is a substantial benefit. Over half of the force (and hence half the structural strength requirement) on regular structures is due to gravity. The structure is tethered, however, and so will have to sustain cantilever wind forces.

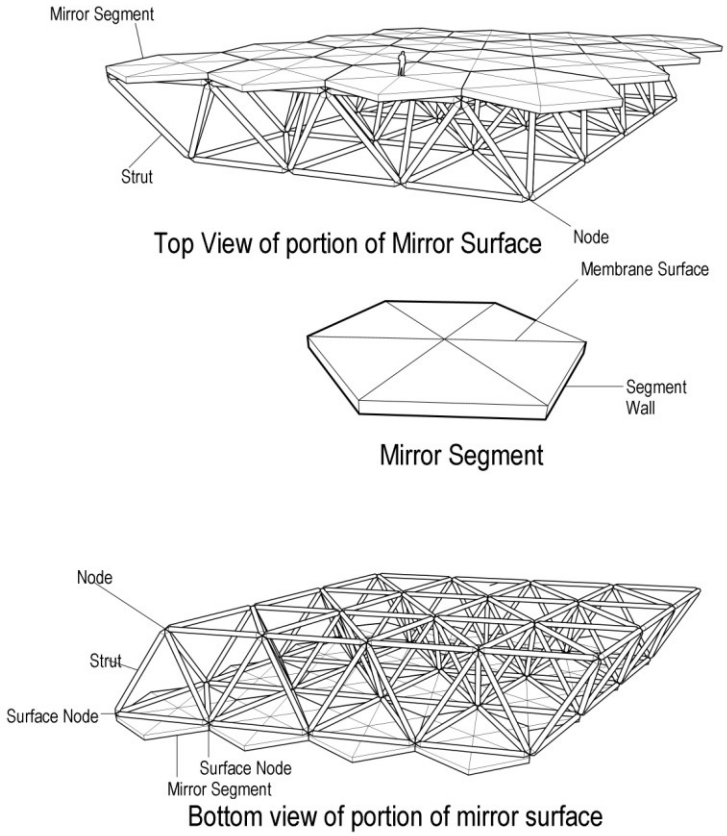

Figure 4

The wind forces in the stratosphere are always light and steady and a fraction of the worst-case ground wind force. The combination of buoyancy effectively canceling gravity and much lighter wind loads results in a practical lightweight structure.

Many truss designs are possible. All minimize the number of unique elements for ease of production and assembly. Struts would be similar in construction to those used in rigid airships and could use aluminum alloy for low cost. The reference design employs a tetrahedral aluminum alloy truss. Figure 4 shows a top view and a bottom view of a small section of the surface truss supporting hexagonal mirror segments. The struts shown are about 17 m long. The hexagonal mirror segments have 10 m sides. Larger struts (not shown), also forming a tetrahedral truss, form the 100 m to 200 m depth of the mirror structure that holds the gasbags.

Unlike blimps, gasbags in rigid structures only have to contain gas. They don't have to provide structural strength or provide protection from weather or the sun. Metalized plastic films can hold unpressurized hydrogen losing only a fraction of a percent a year. A small-diameter hose from the ground attached to the tether/light-pipe can supply hydrogen to replace leakage. Lightweight cords strung across the struts confine gasbags and transmit the buoyancy force to the rigid truss structure. This was the method employed by rigid airships. This allows the gasbags to conform to the truss as they expand from their initial partially filled state. The ozone concentration at 20 km (2.8 ppm) requires care in the choice of plastic material and/or methods to protect it.

Lightweight mirror segments attached with linear actuators to the rigid structural frame accomplish fine pointing accuracy. This is much like how the mirror segments of the Green Bank radio telescope or modern segmented optical telescopes are constructed. However, the accuracy requirements for actively positioning the mirror segments for a solar concentrator are considerably less than those required for the diffraction-limited optics of scientific instruments. Relatively cheap stepper motor linear actuators satisfy the requirements. The mirror segments concentrate the light. They are made of thin, stretched, reflective, plastic membrane over a rigid lightweight frame. The "near space" weather-free environment makes possible the use of thin films. Stretched membrane mirrors have a long history of research and development for ground-based heliostat arrays (Sandia [3], SERI [4], NREL [5]), but the severe weather constraints have meant that sufficiently robust designs cost as much as standard glass and steel heliostats. Very lightweight designs have flown in space (L'Garde [6] [7]), and what is practical in the stratosphere is more akin to space-based designs than ground-based designs.

Light-Pipe Structure:

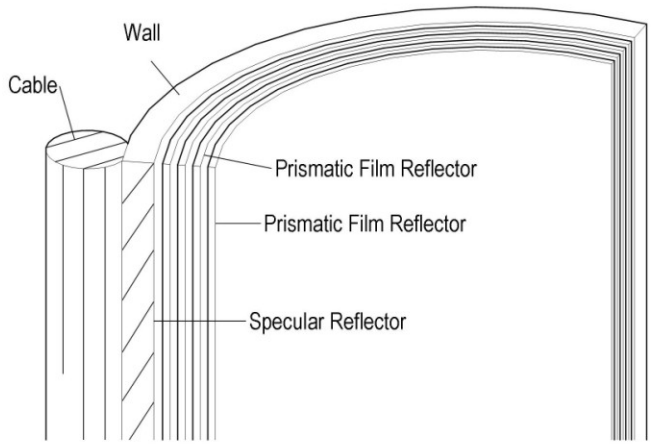

Light Pipe Wall Elements

Figure 5

Figure 5 shows a small portion of a light-pipe wall. The small section shown has one cable, but the full perimeter will have many cables which carry all the light-pipe structural forces. A flexible reinforced fabric wall excludes wind, rain and dirt and provides a gas tight membrane. It also transfers local wind forces to the structural cables. This construction fits within the class of tensioned fabric structures, a mature engineering discipline [8] Birdair, RUBB. The most visible examples of this technology are stadium roofs, such as that of the Georgia dome. There are many more

examples including the Vancouver dome (Figure 23), the Berlin Olympic stadium (Figure 24), and the London Olympic stadium (Figure 22).

Structural and optical system tradeoffs lead to a variety of options for the wall of the hollow light-pipe. Steel cable has the benefit of low risk and low cost. However, steel is heavy, which leads to a larger volume of lifting gas and proportionally more steel due to the effective cable taper required to support the weight of the steel. Analysis shows that using polymer cables such as Kevlar or UHMWPE, which are expensive compared to steel, can be quite close in overall cost due to the insignificant taper and the much reduced buoyancy requirement. The benefit is the ease of construction of the much lighter structure. The quantities of structural polymer required are on the order of several thousand tonnes, which is significant relative to current world manufacturing capacity, so there is price and availability risk. Steel does have an advantage in conducting lightning strikes to the ground.

For a given wind force, the amount of material used in a light-pipe/tether is directly proportional to the diameter. Reduced diameter clearly reduces cost. However, the light-pipe optical efficiency is dependent on the light-pipe diameter in two ways. Firstly, an increased aspect ratio (L/D) leads to more reflections, and secondly, if the concentrator-mirror diameter is constant, the concentration ratio rises as the light-pipe diameter decreases. This increases the divergence angle. This means that the reflectivity of the wall material is crucial. At 99%, diameters of 100 m are appropriate for 1 GWe systems, but at 99.9% 30 m is practical. It's risky to rely on 99.9% without extensive testing. The goal is 30 m for a production system light-pipe.

Another light-pipe issue is the interior gas. Ideally, a sealed pressurized system is best. This maintains the light-pipe shape, excludes dirt and moisture and allows for gases with better optical properties than air. However, this requires transparent membranes. The pressure is low, so the stress in the membrane is low. The optical requirements demand low absorption to avoid heating the material, especially at high light concentrations. Thin plastic membranes easily meet the absorption goals on paper, but constructing such large membranes without absorption hot spots and with reasonable useful lifetimes will be a challenge. Alternatives maintain light-pipe shape with adequate wall hoop strength, and exclude dust and moisture using a small positive pressure maintained by blowers that constantly fill the pipe with dry clean air.

A streamlined shape around the light-pipe decreases wind resistance by up to a factor of ten at a cost of greatly increased complexity.

Concentrator Optical:

The overall concentrator optical system resembles imaging optical systems. There are many alternative designs that meet the goals. The reference design employs an offset parabolic reflector and a matching parabolic collimator with a shared focus. This arrangement is convenient for coupling the light-pipe. The collimator directs concentrated collimated sunlight into the light-pipe. While the optical system resembles imaging optics, the system is inherently a non-imaging system. The accuracies are far from diffraction limited, and the segments are not a single smooth surface but a collection of parabolic

segments with a common focus. The light-pipe is non-imaging and effectively disperses light and produces a uniform energy distribution at the output.

The concentrator and the collimator are actively positioned, segmented-mirror designs. Depending on the light-pipe and receiver designs, the output of the light-pipe at the ground may have an additional concentrator element. Compound parabolic concentrators (CPC) are well suited to this function [9].

Light-pipe Optical:

The light-pipe is a hollow, gas-filled tube with highly reflective walls and (optionally) transparent seals at both ends. The path of light rays from entry to exit is almost exclusively through air or gas. With air cleaned of dust and moisture as the gas, the primary loss mechanism through the air path is from Rayleigh scattering. This loss is about 9.2% from entry to exit. For helium or argon, the loss would be less than 1%.

The light-pipe inner wall shown in Figure 5 is prismatic film 3M 2301, which reflects light using total internal reflection (TIR). The requirement for reflection is for the light to have an incident angle less than the acceptance angle of the reflective material (around 27.6^{o}), hence the requirement for collimated light input. TIR is almost a perfect reflection mechanism. Losses in the prismatic film come from several mechanisms.

1. Absorption within the film, which, because the light path within the film is very short, and the film is very transparent, is small.
2. Scattering from surface imperfections and material impurities, which is very small, and smaller with good quality control.
3. Leakage losses from geometry of the prisms, particularly the radius of the prism apexes. This is the largest mechanism for a single prismatic layer of 1980s era film. This is directly reducible with more accurate prism molding. However, the light that leaks from prism apexes still meets the acceptance angle criteria, so an alternative (or adjunct) to more accurate prisms is a second prismatic film layer to reflect the majority of the leakage, increasing reflectivity substantially. Alternatively, a specular reflective-film second layer, though not quite as good, still enhances overall reflectivity considerably.
4. Dirt accumulating on reflective surfaces. This should be low and manageable with filtering and periodic cleaning if necessary.

Overall, reflectivity (per incident ray) should be on the order of 99.9%, which can reduce light-pipe cost considerably by reducing the diameter. A more conservative 99% reflectivity is still practical, but the light-pipe costs more. The larger cost would still allow commercial electricity generation for less cost than that produced from coal.

The light-pipe wall that acts as the heat sink mostly absorbs the combined losses from Rayleigh scattering and prismatic-film losses. With the cold atmosphere, the wall temperature will not rise significantly. The light intensity at the light-pipe wall is low, so the prismatic film avoids intense UV

exposure. UV management is a major design tradeoff issue. Ideally, UV would not damage the transparent materials. This would allow the UV to contribute to the heat capture. For many plastics, selective UV absorbers or reflectors are the technology currently used to protect films with UV exposure from damage. These work remarkably well, and modern transparent films exposed to direct sunlight are quite resistant to aging effects.

The basic technology for prismatic-film production is roll-to-roll, plastic extrusion molding. This is well established, high-volume, low-cost, manufacturing technology for films, additives, coating technologies and lamination techniques that allow for a wide range of products. For example, recent prismatic film uses a thin polyethylene terephthalate (PET) substrate film with a lamination of molded acrylic prisms to reduce costs and improve optical properties.

More detailed analysis topics

Wind Force:

Wind force is dependent on location and varies seasonally. The Integrated Global Radiosonde Archive (IGRA) [10] [11] is a substantial and important meteorological database that contains wind speed and atmospheric pressure data for 50 years or more for over 2000 sites worldwide. Weather prediction was the original object of this data collection. The data is a highly reliable and public record exceeding 10 GB. It provides wind speed and air density data directly, but not wind force, which is what we are most interested in. Wind force depends on the product of air density and wind velocity squared. We have used the IGRA data to calculate average wind force over a 20 km vertical profile in order to establish accurate statistical confidence levels for wind force. This is a critical input to the design of the light-pipe and the mirror structures. From analyzing the data, it is clear that wind force is very site specific. The 95% utilization averaged wind force varies from 28 Pa to 481 Pa from the lowest wind site to the highest wind site, with a linear distribution for sites between both extremes. There is an assumption that the power plants will go offline and "park" in a safe configuration under extreme weather conditions. Here the assumption is 95% plant utilization.

It is also apparent that the optimal height for the mirror structure is site dependant, and lowers with increasing latitude. It appears that optimal placement is slightly above the tropopause. 20 km works well for northern California.

Table 1 shows an example of the analyzed wind force data for the Oakland, California site. The column marked "#" shows the number of valid records used for the corresponding row statistics. All other columns are wind pressure in Pa. The "%" columns represent the average pressure exceeded by that percentage of samples. For example from the "ALL" row the average of the highest 5% of the wind pressures is 239.8 Pa. The maximum average wind force recorded for Oakland is 525.9 Pa and occurred in December 1971.

The monthly data shows seasonal variability and the yearly data shows long-term variability.

Based on this statistical data we can generate a vertical wind profile for the desired operational confidence level for the desired site and use that in the design of the light-pipe and mirror structure.

Station name: OAKLAND US
Station location: lat 37.75, long -122.22 station geometric elevation: 6 m
0-20 km average wind force

Table 1 **Light-pipe wind force**

when	#	avg	std	min	10.00%	5.00%	2.00%	1.00%	0.50%	max
Jan	581	96.87	67.08	1.5	234.8	261.5	294.9	327.9	367.2	401.6
Feb	577	91.2	64.95	5.2	230	254.9	278.6	293.2	302.7	323.1
Mar	577	85.48	59.73	1.2	211.2	240.5	275.1	301.4	326.2	379.2
Apr	568	91.54	64.9	2	229.9	256.1	285.3	298.9	309.8	324.2
May	584	76.43	59.97	1.5	207	237.6	269.2	296	326.8	336.8
Jun	539	58.68	45.15	0.2	153.8	178.2	207.9	238	264.5	304.6
Jul	585	38.64	32.68	0.6	111.6	133.9	157.3	173.1	183	185.2
Aug	564	42.74	32.74	1	117.3	135.9	153.6	160.5	171.2	182.6
Sep	538	49.16	41.08	1	137.5	154.1	174.3	185.6	186.6	189.6
Oct	564	66.21	56.79	0.7	194.3	227.7	276.3	303.4	327.3	343.3
Nov	577	100.58	65.15	3.5	236.2	267.4	304.4	335.8	366.1	400.2
Dec	597	90.81	69.57	4	239	280	344.3	404.6	466	525.9
1970	100	104.07	89.28	5.4	302.4	355.9	391.6	400.2	400.2	400.2
1971	24	162.38	130.16	10.7	463.8	525.9	N/A	N/A	N/A	525.9
1972	27	107.05	72.31	13.9	228.8	234.6	234.6	N/A	N/A	234.6
1973	29	128.82	73.18	9.5	271.6	289.1	289.1	N/A	N/A	289.1
1974	7	92.96	106.51	14.2	264.7	N/A	N/A	N/A	N/A	264.7
1975	30	133.98	79.48	12.6	287.8	319.2	355	N/A	N/A	355
1976	78	82.92	62.69	6.2	219.7	233.3	241.8	248.6	N/A	248.6
1977	52	103.59	86.24	6.6	307	332	379.2	379.2	N/A	379.2
1978	33	108.96	110.21	9	376.1	413.8	489.1	N/A	N/A	489.1
1979	27	104.88	79.99	4.7	245.3	275.5	275.5	N/A	N/A	275.5
1980	35	89.77	55.17	1.5	199.4	227.8	236.7	N/A	N/A	236.7
1981	8	106.09	52.74	20	181.9	N/A	N/A	N/A	N/A	181.9
1982	9	88.37	69.45	4.6	199.5	N/A	N/A	N/A	N/A	199.5
1983	4	107.83	37.07	52.5	N/A	N/A	N/A	N/A	N/A	130.3
1984	11	65.45	45.37	17.6	178.2	178.2	N/A	N/A	N/A	178.2
1985	32	62.86	64.69	6.6	215.6	242.8	300.1	N/A	N/A	300.1
1986	35	69.62	63.65	0.2	185.8	201.2	226.3	N/A	N/A	226.3
1987	90	74.7	66.6	2.6	210.2	228.3	239.3	246.2	N/A	246.2
1988	97	81.06	67.34	2.3	230.1	267.9	304.2	309	N/A	309
1989	63	89.84	56.5	5.7	203.1	228.4	242	242	N/A	242
1990	509	77	59.96	2	206.9	243	278.9	299.7	314.8	343
1991	509	68.31	61.54	1	208.8	241.6	268.6	282.8	290.7	305.1
1992	425	61.57	50.23	1	172.2	192.6	214	232.6	238.7	240.6
1993	430	73.9	51.07	0.7	178.4	199.9	236	263	277.7	282.4
1994	471	71.08	53.58	1.2	187.2	215.3	260.9	281.3	314.4	342.6

1995	497	71.26	55.53	2.4	192.6	221.4	248	263.7	267.8	268.3
1996	497	76.64	62.21	0.8	215.1	243.4	277.9	304.4	335.7	336.8
1997	513	76.9	63.36	0.6	216	244.8	280.7	298.3	308.3	324.2
1998	557	78.94	61.54	1.2	211.1	242.3	272	285.9	302.9	326.9
1999	512	67.32	55.64	1.3	191.6	213.6	240.5	256.7	267.2	304.7
2000	540	68.67	54.7	0.9	191.1	215.6	239.7	258.4	268.7	286.2
2001	600	68.1	52.67	0.3	185.6	214.1	250.2	278.6	315.5	393.8
ALL	6851	74.33	60.45	0.2	207.4	239.8	278.2	307.2	339.6	525.9

Table 2 shows the IGRA-derived wind force for 20 km altitude, which determines the force on the mirror structure. There are more years covered for this table because more samples met the simpler criteria. From the "ALL" row the wind force that is exceeded 5% of the time is 23.4 Pa. The criteria for wind samples for 20 km include the nearest sample within 2 km of 20km. This results in the acceptance of some samples as low as 18 km. These samples account for the exceptional high wind forces in the max column, and highlight the necessity of monitoring winds and keeping the mirror structure above the occasional exceptional high-altitude troposphere wind. For example the exceptional wind force on one occasion in September 1985 was for a sample near 18km.

Oakland 20 km wind force.

Table 2 Collector wind force

when	#	avg	std	min	5.00%	2.00%	1.00%	0.50%	0.20%	0.10%	max
Jan	2918	3.66	5.54	0	21.3	30.1	38.5	49.2	69.5	89.3	96.3
Feb	2767	3	5.2	0	18.3	25.9	33.6	43.3	61.1	87.5	165.9
Mar	3026	2.94	4.87	0	18.8	28	35.9	44.1	60.2	74.1	86.5
Apr	2967	2.29	4.09	0	15.3	24.5	32.5	40.1	48.6	55.6	73.3
May	3091	0.99	2.51	0	6.8	11.4	17.1	26.4	45.8	58.2	85.1
Jun	3067	1.24	2.78	0	5.8	8.7	12.3	19.1	36.5	63.3	135.3
Jul	3251	2.13	1.57	0	6.1	7.3	8.4	10	12.9	18.3	33.2
Aug	3125	1.53	1.81	0	5.5	7.4	9.5	12.4	20.9	32.8	73.8
Sep	3031	1.08	8.17	0	7.8	14.2	23.6	41.2	90.4	166.1	390.8
Oct	3098	1.89	3.26	0	9.9	14.1	18.8	26.3	42.1	61.9	130.9
Nov	2777	3.28	4.95	0	17.4	24.8	32.2	42.3	60.4	87.6	140.8
Dec	2883	3.91	21.21	0	27.4	46.8	72.3	118	224.6	404	404
1948	44	2.11	2.58	0	10.5	13.3	N/A	N/A	N/A	N/A	13.3
1949	33	2	2.01	0	8.4	8.9	N/A	N/A	N/A	N/A	8.9
1950	12	2.67	2.04	0	5.9	N/A	N/A	N/A	N/A	N/A	5.9
1951	7	1.93	1.09	1	N/A	N/A	N/A	N/A	N/A	N/A	4
1952	12	2.09	2.11	0	5.7	N/A	N/A	N/A	N/A	N/A	5.7

1953	12	2.74	2.17	0.2	6.7	N/A	N/A	N/A	N/A	N/A	6.7
1954	101	2.17	2.44	0	10	11.8	13.1	13.1	N/A	N/A	13.1
1955	763	2.79	3.84	0	15.3	22.3	28.1	33.9	39.4	42.3	42.3
1956	733	2.02	2.22	0	8.8	10.7	12.1	13.3	20	20	20
1957	721	2.67	4.23	0	17.1	25.7	33.2	37.5	51.6	51.6	51.6
1958	545	1.48	1.64	0	6.8	9	10.6	11.3	13.1	13.1	13.1
1959	630	1.87	2.27	0	8.9	11.9	14.7	16.6	18.3	18.3	18.3
1960	611	2.13	2.35	0	9.8	12.5	14	15	16.4	16.4	16.4
1961	661	2.49	3.95	0	16.2	23.8	29	36	44.8	44.8	44.8
1962	672	2.11	2.71	0	11.2	14.3	15.9	19	22.9	22.9	22.9
1963	662	3.67	5.88	0	24.5	32.3	36.8	45.1	51.7	51.7	51.7
1964	667	1.96	2.93	0	12.3	17.2	19.5	22.2	24.3	24.3	24.3
1965	679	2.16	3.88	0	15.3	24.9	30	31.8	33	33	33
1966	666	2.39	4.34	0	15.2	23.5	31	46.7	75.3	75.3	75.3
1967	684	1.97	3.01	0	11.3	16.3	22.1	32.2	38.4	38.4	38.4
1968	685	2.7	17.52	0	27.2	55.2	98.3	189.9	189.9	189.9	189.9
1969	688	2.63	5.18	0	19.9	27.8	35.8	50.9	86.5	86.5	86.5
1970	688	2.15	2.42	0	9.6	12.5	15.2	18.5	22	22	22
1971	609	2.51	4.67	0	17	27.4	36.9	47.3	73.3	73.3	73.3
1972	605	2	2.36	0	9.4	13.4	16.8	18.6	21.3	21.3	21.3
1973	522	1.96	6.56	0	14.8	27.9	44.4	63	140.8	140.8	140.8
1974	442	1.77	2.37	0	10.1	13.2	16.1	20.2	21.6	N/A	21.6
1975	633	1.89	2.83	0	11	15.9	21.7	27.3	36.5	36.5	36.5
1976	692	1.45	1.79	0	6.9	9.8	13.4	18.1	23.4	23.4	23.4
1977	666	1.69	2.13	0	8.4	11.5	14.1	18.2	21.9	21.9	21.9
1978	662	2.38	4.74	0	18.7	28.7	35.9	46.9	50.9	50.9	50.9
1979	663	1.79	2.1	0	8.6	10.7	11.6	12.8	14.9	14.9	14.9
1980	660	2.09	3.78	0	15.2	22.3	28.4	35.6	43.3	43.3	43.3
1981	650	2	2.85	0	11	16.2	19.9	25.9	32.5	32.5	32.5
1982	593	1.79	2.34	0	9.2	11.8	14.1	17.4	24	24	24
1983	565	1.85	3.02	0	11.4	18.2	24.3	31	32.8	32.8	32.8
1984	629	2.33	4.13	0	14.7	23.7	34.7	46.8	58.5	58.5	58.5
1985	618	4.55	44.8	0	53.1	114.1	208.8	390.8	390.8	390.8	390.8
1986	565	1.7	2.37	0	9.7	13.7	16.2	19.1	23.1	23.1	23.1
1987	644	1.84	5.14	0	13.6	24.7	42	68.4	85.1	85.1	85.1
1988	595	2.13	3.17	0	13.2	17.4	20.1	22.5	24.3	24.3	24.3
1989	528	1.93	2.37	0	9.8	12.6	14.5	15.7	18.7	18.7	18.7
1990	701	2.68	3.99	0	16	24.5	30	34	40.7	40.7	40.7
1991	692	2.75	4.8	0	19.9	28	35	43.8	49.4	49.4	49.4
1992	625	2.84	7.12	0	26.3	40.9	57.7	77.5	96.3	96.3	96.3
1993	621	1.93	2.22	0	8.8	10.4	11.4	12.4	13.6	13.6	13.6

1994	617	2.44	3.31	0	13.4	17.8	21	21.9	22.6	22.6	22.6
1995	669	2.07	3.01	0	10.7	15.7	20.8	32.1	47.6	47.6	47.6
1996	660	2.78	6	0	16.8	26.5	37.7	65.1	130.9	130.9	130.9
1997	683	2.06	2.91	0	12.2	16.4	18.2	20.8	25.9	25.9	25.9
1998	667	3.26	3.93	0	16.6	22.1	25	27.8	29.1	29.1	29.1
1999	673	2.35	5.86	0	14.5	25.7	38.3	65.4	135.3	135.3	135.3
2000	671	2.09	3.08	0	12.3	18.7	22.9	27.9	31.4	31.4	31.4
2001	748	2.1	2.74	0	11.3	15.1	18.8	21.1	23.8	23.8	23.8
2002	632	2.58	7.35	0	17.2	30.2	52	83.1	165.9	165.9	165.9
2003	672	1.88	2.43	0	9.3	12.8	15.7	21.4	33.7	33.7	33.7
2004	612	1.99	2.83	0	11	15.6	20.1	26.3	36.3	36.3	36.3
2005	626	1.9	2.7	0	11.2	15.2	18.6	22.5	29	29	29
2006	720	3.43	5.22	0	19.3	26.8	34.4	42.3	75.1	75.1	75.1
2007	699	1.47	2.42	0	8.7	13.7	19	26.8	35.4	35.4	35.4
2008	680	2.59	5.29	0	21.5	33	39.7	48.9	60.3	60.3	60.3
2009	672	3.64	4.74	0	19	27.2	33	36	40.8	40.8	40.8
2010	144	2.34	2.87	0	12	14.8	18.2	18.2	N/A	N/A	18.2
ALL	36001	2.3	7.42	0	14.9	23.4	32.6	45.4	72	107.5	390.8

In recent years interest in high altitude airships (HAA) for surveillance and communication has led to investigation of winds at 20km altitude. Work based on the NCAR/NCEP reanalysis data which includes satellite Doppler wind measurements going back to 1979 [(12)] is consistent with the IGRA data analysis and provides insight into the sources of stratospheric wind variability. In the analysis cited above, winds never exceed 50 ms, and match the IGRA statistical profile.

Direct sunlight intensity:

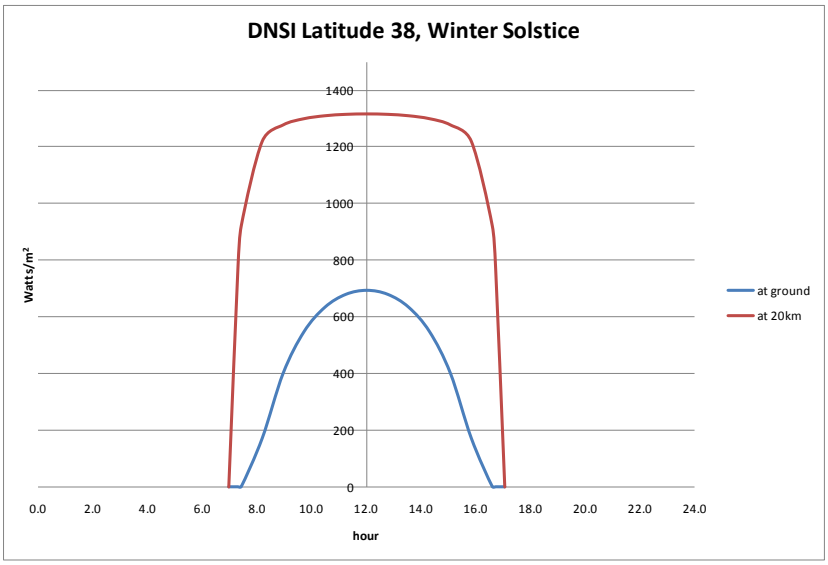

Figure 6

Sunlight and its interactions with the atmosphere are well understood, and accurate models exist that can predict absorption and scattering through the atmosphere (e.g. MODTRAN). We have adapted a simplified model from Young [13] that, given azimuth angle, calculates relative air mass accounting for diffraction. We calculate azimuth angle given the latitude, the day and the hour. Then we calculate relative air mass for ground level and 20 km altitude. This then allows us to calculate direct sunlight in Watts/m^2. The target location for the first StratoSolar prototype system is northern California, so we use Latitude 38 as a relevant example. Figure 6 is a graph of light intensity for latitude 38 on the winter solstice. The horizontal axis is hour, with noon at 12.0. The vertical axis is direct normal solar insolation (DNSI) in Watts/m^2. The red line is sunlight through the day at 20 km. The blue line is sunlight at the ground with clear skies. Integrating the areas under the curves gives daily Wh/m^2 of incident solar energy. For this case at 20 km, this is 15,323 Wh/m^2, and at ground level, this is 7,210 Wh/m^2. For the summer solstice, the numbers are 18,880 Wh/m^2 and 10,169 Wh/m^2.

At higher latitudes, the difference between summer and winter is much more pronounced, and the difference between energy at 20 km and the ground is even more pronounced. For latitude 60, the numbers are 6,202 Wh/m^2, 304 Wh/m^2 at winter solstice and 22,219 Wh/m^2, 10,917 Wh/m^2 at summer solstice.

For latitude 38, integrating over the year gives an average of 2.13X more light at 20 km altitude than at the ground. However, yearly average does not really describe the advantage. The winter solstice is 2.77X better. In addition, real ground-based systems don't always have clear skies, and need to have a minimum sunlight level before operating. NREL gathered ground level sunlight intensity data for the US for 30 years, which shows the real advantage is at least 3X, and at higher latitudes, it is considerably more.

Sunshape:

The other important attribute of sunlight as it enters the light-pipe is its dispersion angle. The fact that sunlight is highly collimated and has a small dispersion angle is what allows the practical use of a light-pipe. This dispersion angle is actually a distribution of angles between the solar rim angle of 4.653 mrad and 0 mrad. For simplified calculations, an average angle is required. The ideal solar disk has a flat

energy distribution. The real solar disk darkens near the edges. This is due to solar atmospheric scattering. The radius of the solar disk from which sunlight is emitted determines the angle of received solar energy. Simple analysis just assumes all solar radiation has the rim angle of the solar disk, 4.653 mrad, which is pessimistic. There is more area at larger radii, so the average radius is more than half. However, larger radii have less energy, so the average angle is dependent on both area and W/m^2 at the solar surface. We have performed an area and emissivity weighted calculation with data from (Rabl and Bendt, 1982), which produces an average angle of 2.79 mrad. An area-weighted flat emissivity produces an average angle of 3.2 mrad. The 20 km average is higher than 2.79 mrad. It is clearly less than 3.2 mrad, 3.0 mrad is probably a conservative estimate.

Light entering the solar concentrator has an average angle of 3.0 mrad. The average angle on exit from the concentrator and entry into the light-pipe depends on the concentration ratio of the optical concentrator. This can be calculated from $C=\sin^2\Theta'/\sin^2\Theta$, where C is concentration ratio, Θ is the average dispersion angle at the entry aperture of the concentrator, and Θ' is the average dispersion angle at the concentrator exit aperture [14] [15] EOLSS. For example for C=100, the average dispersion angle of the concentrator output is 30 mrad. This average dispersion angle of concentrated sunlight and the geometry of the light-pipe, determines the number of light traversals down the length of the light-pipe. We have developed tools to study tradeoffs in light-pipe geometry, concentration ratio and light-pipe-wall reflective efficiency.

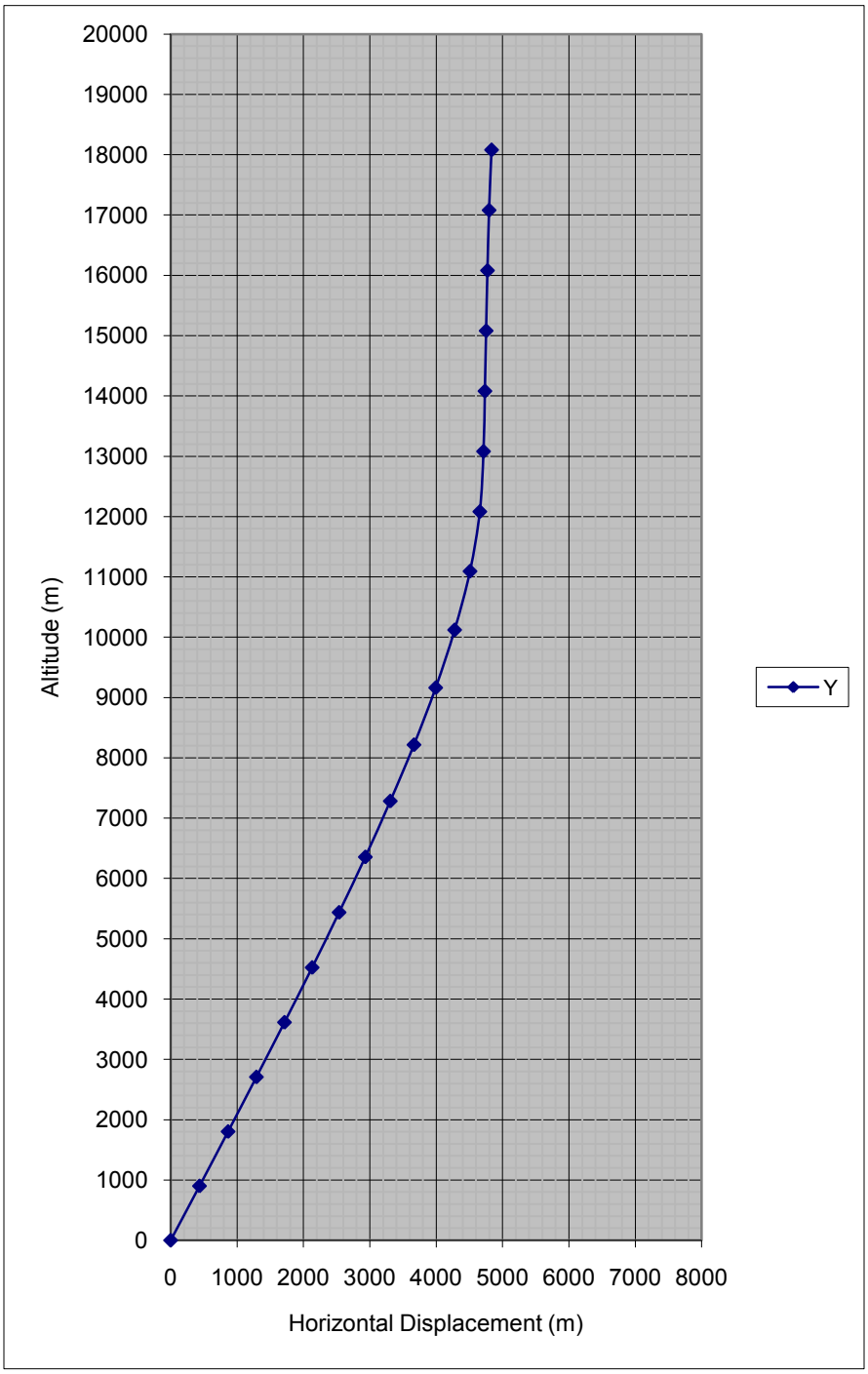

Figure 7

Light-pipe under wind load:

The graph shown in Figure 7 shows the result of a simulation of a prototype system light-pipe subjected to a 95% wind load based on the Oakland station wind data. The wind is at or below this load 95% of the time. The design assumes the following parameters. The collector mirror radius is 163 m. The radius of the light-pipe is 15 m. The top 5 km of the light-pipe has an outer sleeve of radius 115 m containing hydrogen-filled gasbags attached to the light-pipe and providing buoyant lift force. The light-pipe wall includes vertical polymer cables that carry the buoyancy and wind-induced forces. The light-pipe wall is a smooth and airtight structure formed from structural fabric.

The 2D calculation models the light-pipe as 20 rigid segments connected by pin joints. The calculation is iterative. The wind force on each segment is calculated and depends on the angle of the light-pipe and the altitude. It also depends on the coefficient of drag, wind velocity and air density. Buoyancy and weight for each segment are also calculated. The wind force for segments changes with altitude and updates iteratively. The desired maximum deflection sets the required amount of buoyancy.

The goal of the simulation is to verify the practicality and the cost of the solution. The quantities of two materials dominate the cost, the cables and hydrogen gas. For this simulation, 3,129 tonnes of polymer cables are required at $20/kg for a total of $62,585,607. The hydrogen required is 1,842 tonnes at $6/kg for a total of $11,053,712. For a steel cable solution, 29,142 tonnes are required at a cost of $1.5/kg and 3,425 tonnes of hydrogen at $6/kg for $20,554,423. A steel solution costs a total of $64,268,806. A polymer cable solution costs a total of $73,639,319. The steel solution is cheaper but is considerably heavier. Heavier steel and a larger volume of hydrogen will be more difficult to handle during construction. This is typical of engineering analysis. Even this simple model allows evaluating a wide variety of options and tradeoffs.

Accurate models for the aerodynamic behaviors of cylindrical towers also allow the calculation of vortex-shedding induced forces [(16)]. These are high frequency and low amplitude. Asymmetric aerodynamics of a structure cause the more dangerous “galloping” forces. For example, asymmetric ice buildup causes galloping in the case of power cables. The light-pipe is inherently symmetrical, and ice buildup should not distort the aerodynamics significantly. Ice is dangerous in other ways, and anti-icing systems are a likely part of the engineering solution.

This is a simple static model. It is possible, using engineering software tools, to simulate the system with an accurate meteorological wind model that then drives a simulation of the aerodynamic and dynamic behavior of the structure. This is one of the goals of the funded R&D stage. Accurate computer simulation can test and verify much of the risky engineering.

The current simulations show that for a small prototype system the light-pipe is the dominant cost element. The optical efficiency of the light-pipe dictates the minimum practical diameter. As systems scale, the light-pipe cost scales with the square root of the size of the collector and is proportionately a much smaller cost.

Light-pipe optical system details:

From an optical perspective, the light-pipe is a hollow, gas-filled tube with reflective walls and (possibly) transparent seals at both ends. This optical system analysis covers light interactions with the gas path (primarily Rayleigh scattering), the reflections from the wall (prismatic-light-film), and the transparent seals (absorption, reflectivity, and physical strength). We have already covered the energy intensity of the concentrated sunlight entering the light-pipe, and its angular dispersion (sunshape).

Prismatic film:

Table 3

Prisim Light Guide						
		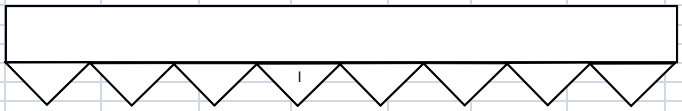				
					polycarbonate	polycarbonate
					3M OLF	bigger prisms
		l optimum = ((4*r*(1-(1/n^2))^.5)/k)^.5		0.012209472	0.00682426	0.003939988
		r is prism apex radius		5.00E-06	1.50E-06	5.00E-07
		n is prism material refractive index		1.5	1.586	1.586
		k is attenuation per unit length of prism material		0.1	0.1	0.1
		t = overall thickness = h+i			0.000686	0.0006
		h = prism height =l/2			0.000178	0.0005
		i = base height			0.000508	0.0001
		l = prism width			0.000356	0.001
		sin^2(22.5)			0.15	0.15
		theta max (radians) = cos-1(((1-n^2*sin^2(22.5))/(1-sin^2(22.5))))^.5			0.54	0.54
		theta max (degrees)			30.66	30.66
		weight (kg/m^2)			0.5	0.7
		max temp (degrees C)			129.4	129.4
		R=guide radius			80	80
		D			101.8592496	101.8592496
		D is average cross sectional distance travelled by a ray in crossing the guide air space.				
		For a circular guide, D=(4*R)/pi				
		Polycarbonate is affected by UV radiation in the 300nm to 350nm range.				
		Traditionally UV absorbers are added to or layered on the polycarbonate surface to reduce this problem.				
		Adding UV absorbers to the Concentrator surface is better in this case.				
Attenuation per unit length for a light pipe is = (2/3)*(theta max/D)*(((4*r)/l) +((k*(l+2*i))/(1-(1/n^2)))					5.98E-05	7.70E-06
		L			20000	20000
		Attenuation			1.20E+00	1.54E-01
		Transmittance			-20%	85%
This equation assumes light is evenly distributed between 0 degrees and theta max. Collimated sunlight will have a much narrower range of angles.						
Attenuation per traversal is two terms						
Prism loss	ap=4*r/l				1.685%	0.200%
dielectric attenuation	ad=(k*(l+2*i))/(1-(1/n^2))^.5				0.018%	0.015%
Total attenuation per traversal=ap+ad					1.703%	0.215%
Traversals per unit length = tan theta/D					0.000171347	0.000171347
Total traversals = traversals per unit length * L					3.426940183	3.426940183
Reflectance per traversal					98.297%	99.785%
Add a mylar reflecting backing layer	95%				99.898%	99.975%
prism loss with mylar backing					8.43E-04	1.00E-04
Two approaches to higher reflectivity						
First is use larger prisms, assuming that apex radius cannot be reduced. This reduces prism loss but raises dielectric attenuation.						
Second is to use a conventional reflector in addition to the prisms. A reflective coating covering the prisms apex would reduce the prism losses.						
This would involve applying coatings in strips two micrometers wide.						
Alternatively simply using a reflective backing layer would reflect light that escaped from the prism apexes.						

Table 3 above is extracted from a larger spreadsheet. It shows the basic calculations for designing a prismatic film. Whitehead describes this in detail in [17]. 3M licensed the technology and used it to develop its optical light film (OLF) product in the 1980s [18]. This product has had some success in commercial lighting, for which it was developed and optimized. The second column from the right in the table above shows the calculations for OLF. Prismatic film reflects light using total internal reflection

(TIR). This mechanism is almost 100% efficient. In a light-pipe, the OLF flat surface is the inner surface where light enters the film, and the axis of the prisms is aligned along the optical axis of the light-pipe. Only light that satisfies the acceptance angle criterion is reflected. For OLF this angle is 27.6°. Light enters on the flat side and refracts inward. It encounters a prism wall where it is reflected by TIR. It traverses the prism and is reflected by TIR back out at the second prism wall, meets the flat wall and refracts back into the light-pipe. Geometry guarantees reflection for light within the acceptance angle.

The major loss elements are dielectric absorption in the OLF plastic material and leakage through the finite radius prism apexes where the geometrical requirements for TIR are not satisfied. OLF achieves 98% plus reflection efficiency. As can be seen from the calculations in the table above the apex loss is dominant for OLF, 1.68% vs. .018% for dielectric loss. Whitehead has shown that refractive losses at the apexes are minimal [19]. Mie scattering from material contaminants and surface defects are also minimal.

Recent prismatic films have used a laminate with a PET base layer and acrylic prisms (Microsharp Corp.). The far right column of the table above shows an example of such a material optimized for StratoSolar. The reflectivity improves by widening the prism base width and/or reducing the radius of the prism apexes. The example shown does both, and improves reflectivity to 99.8%. Alternatively, or in combination, given that the major loss mechanism is apex leakage where the leakage light still meets the acceptance angle criteria, a secondary reflector behind the prism apexes will reflect the "leaked" light back into the prisms, where the optical geometry then ensures it refracts back into the light-pipe. The secondary reflector can be a specular reflector such as aluminized Mylar, or a second prismatic film layer. This second layer improves OLF to 99.9%, and the PET-based laminate film to 99.97%. At these levels of efficiency all the secondary loss mechanisms assume a higher importance. High-quality materials and manufacturing to reduce scattering particulates and surface defects are important. It's important to excluding particulates from within the light-pipe that accumulate on the reflecting surface. Routine cleaning may be necessary. Automated cleaning machines can accomplish this conveniently during the hours of darkness.

Rayleigh scattering:

The light path through the light-pipe is predominantly through the interior gas. The dominant loss mechanism along this path is Rayleigh or molecular scattering, which scatters the light such that the majority of the scattered light no longer meets the acceptance angle criterion. Using the standard "Extraterrestrial Solar Irradiance (WRC Spectrum) in Increments of Wavelength" as a reference solar input, and a model from Gueymard [20] for Rayleigh scattering transmittance, and assuming clean dry air as the gas, we calculated the transmittance through the light-pipe section as 90.5%. The transmittance for hydrogen is 97.2%, and for helium is 99.92%. However the buoyancy-induced pressure within the light-pipe for hydrogen and helium would demand a much stronger light-pipe and top and bottom transparent seal membranes. Dry air is the most convenient option. A neutral buoyancy argon/hydrogen mix would be another relatively low cost and high efficiency option.

Light-pipe Seal Optics:

A simple version of the light-pipe maintains its shape with internal pressurization in the region of 500 Pa. This requires that the light-pipe be airtight, and particularly that the ends be both airtight and transparent. In one example, the ends are thin bi-ax PET film, 1 mm thick with anti-reflective coatings. Absorbance is typically around 10% per m for PET, polycarbonate or acrylic. One mm is thick for bi-ax PET film. Assume the light intensity is 200 kW/m^2 at the light-pipe input. This would result in 20 W/m^2 being absorbed. That's 0.002 W/cm^2. Natural convection should cool this small heating effect, but fans could keep air moving if necessary. These transparent seals could experience intense UV which might degrade the film over time. One solution is to absorb UV using absorption additives [21] on a coating applied to the mirror surfaces prior to light entering the light-pipe. Another solution is a selective UV reflective coating applied to the seals along with the antireflective coating.

From the boiler equation, stress in the film = P*R/t = 500*50/0.001 = 25 MPa, well below the limit for PET. Bi-ax film has a yield-strength of 190 to 260 MPa. A thin web of cables could add reinforcement across the window if thinner film or higher pressure were desired. The trick would be to make them reflective so as not to heat the film.

Light-pipe overall design:

2*R	163	133	103	73	33
D	104	85	65	46	21
Divergence half angle (degrees)	3.77E+00	4.62E+00	5.97E+00	8.46E+00	1.92E+01
Divergence half angle (radians)	6.59E-02	8.07E-02	1.04E-01	1.48E-01	3.35E-01
Traversals per unit length = tan theta/D	6.36E-04	9.54E-04	1.59E-03	3.19E-03	1.62E-02
Total traversals = traversals per unit length * L	1.27E+01	1.91E+01	3.18E+01	6.38E+01	3.24E+02
Light pipe wall efficiency 1	80%	72%	58%	33%	0%
Light pipe wall efficiency 2	97%	96%	93%	87%	50%
Light path length	20043	20065	20108	20217	21094
Light pipe wall efficiency 1 average dispersion	90%	85%	76%	58%	6%
Light pipe wall efficiency 2 average dispersion	99%	98%	97%	93%	71%
Light pipe wall efficiency 1 average dispersion with 2nd reflective layer	99.35%	99.03%	98.39%	96.80%	84.78%
Light pipe wall efficiency 2 average dispersion with 2nd reflective layer	99.84%	99.76%	99.60%	99.19%	95.96%
Wall Surface absorbtion % of entry intensity	0.00264%	0.00323%	0.00417%	0.00591%	0.01342%
wall surface incident radiation % of entry intensity(R/2*L)*T	2.59%	3.17%	4.09%	5.80%	13.17%
Light pipe entry intensity (W/m^2)	2.00E+05	3.00E+05	5.00E+05	1.00E+06	5.70E+06
Wall absorbtion intensity (W/m^2)	5.27E+00	9.69E+00	2.09E+01	5.91E+01	7.65E+02
Relative air mass ma	1.00	1.00	1.01	1.01	1.05

Table 4

As has been discussed earlier, the overall efficiency of the light-pipe is a function of several variables. These include: the radius R, the length L, the concentration factor C, the wall reflectivity efficiency and Rayleigh scattering losses through the length of the optical path. Table 4 above shows the resulting light-pipe efficiencies for a variety of choices. Two assumptions are: the primary mirror aperture has a diameter of 2,300 m, and the light-pipe has a length of 20 km. The row labeled "2*R" is the light-pipe diameter. As the light-pipe diameter decreases, the concentration factor rises. The columns represent different light-pipe-diameters, and hence different concentration ratios. The row labeled "D" calculates the average light-path horizontal traversal length. The row "divergence half angle" calculates the maximum divergence angle of the light at the light-pipe entry aperture. The rows "Traversals per unit length" and "Total traversals" are then calculated. The overall resulting efficiency of the light-pipe for six cases of light-pipe-wall reflectivity is calculated. The wall absorption in W/m^2 is also calculated. This analysis does not include Rayleigh scattering losses, which will depend on the gas within the light-pipe.

These calculations show that with concentration factors of 100 or 200, relatively poor wall-reflection efficiency is acceptable. With increasing concentration factor, the light-pipe wall reflection efficiency needs to rise to enable practical light-pipes. The six cases of wall reflectivity show the technical steps to increase prismatic-film reflectivity discussed in the “prismatic film” section. These include altering the prism size and apex radius, and adding a secondary reflective layer.

Miscellaneous topics

Ground elements

The ground elements of the system are not the focus of this document. No innovation in this area is necessary to prove the viability of StratoSolar. The ground elements do represent the major components of cost in a complete electricity generation system, and we have investigated how best to exploit the benefits of the StratoSolar approach. Much of the technology such as turbo-generators is standard or has been exhaustively studied and developed over many decades. Most solar receivers to date have used standard steam-boiler technology. Compared to other CSP systems, with the StratoSolar approach there is more flexibility in physically arranging the receiver, storage and turbine generators. The receiver can be one large receiver at ground level, as opposed to multiple receivers on top of tall towers. This means that large-scale turbo generators developed for utility scale power plants are directly applicable. R&D to improve and develop utility scale turbo-generators, such as high temperature Brayton cycle turbines is also directly applicable [(22)]. This makes StratoSolar a more natural evolutionary technology than other CSP and alternative energy approaches.

Thermal storage is a necessary part of a solution to deliver electricity 24/7. We have conceived a thermal storage solution that is low cost, low risk, and highly flexible which we discuss in more detail below.

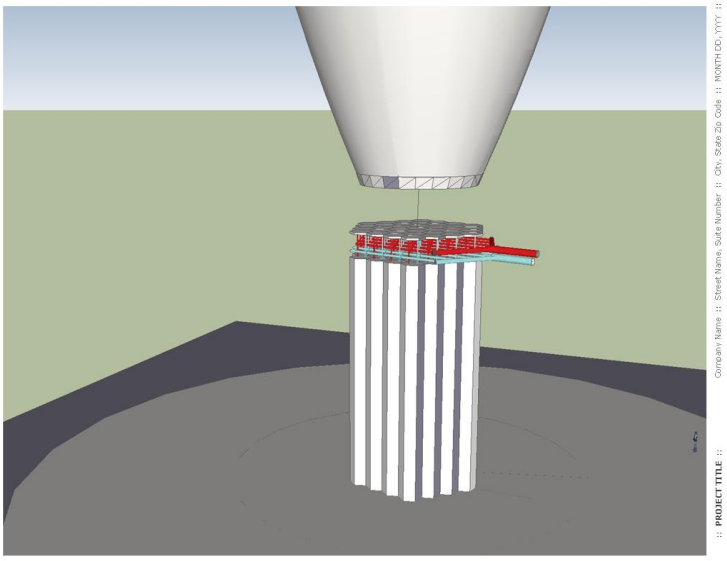

Figure 8

The ground system elements are:

1. A final stage concentrator. This may not be necessary for all configurations.
2. A cavity
3. A receiver
4. Thermal storage
5. Turbo generators and other standard power-plant equipment.

Figure 8 and Figure 9 show an example of the various ground elements. The top element is the exit aperture of a final stage CPC concentrator. The transparent membrane at the exit of the light pipe is at the entry to the CPC. Convective cooling protects the transparent membrane and the upper portion of the CPC. Neither absorbs significant outgoing radiation from the receiver. Cold clean air circulates from the top of the CPC down through the cavity space above the receiver where it exits through the bottom of the reflective cavity walls. This can be an open or a recirculating closed cooling

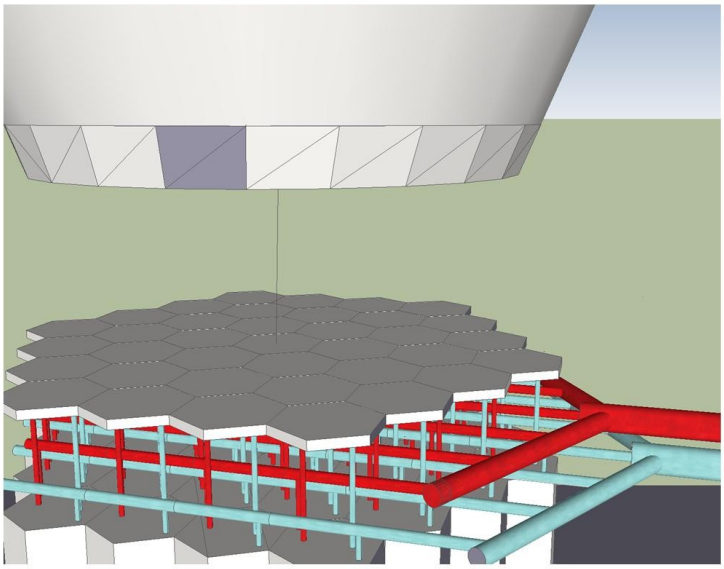

Figure 9

system. Alternatively, an inert gas like argon, which is cheap and readily available, provides an oxygen-free, convection-cooling environment. Significant radiation energy from the hot receiver heats the bottom portion of the CPC. This may necessitate heat resistant material such as reflective stainless steel cooled with water. Light exits the CPC and impinges upon an array of hexagonal flat-plate receivers. Having multiple small receivers accommodates variations in solar incident radiation. The receiver, the turbo generator and other power plant equipment are at ground level. The flow rate of coolant through each receiver element is adjustable via its individual circulating pump. It also facilitates mass production of receiver elements. Two short vertical pipes connect each flat plate receiver element to a below ground thermal storage element. The blue pipe carries the incoming cold heat-transfer fluid to the receiver element, and the red pipe carries the outgoing hot fluid that charges the storage element. The tall vertical hexagonal containers are the thermal storage elements. The pipe cascade shown connects the array of successively larger diameter pipes forming the thermal discharge circuit. This terminates in the large-diameter, blue cold-input pipe and the red hot-output pipe on the right of the diagram. These pipes connect to the turbo generator (not shown) directly if it is a helium turbine. Otherwise, as with existing nuclear reactors, they connect to a heat exchanger that heats steam to drive a Rankine cycle turbine. For clarity, this diagram also does not show the reflective cavity wall.

Thermal storage:

The current R&D focus in thermal storage for CSP plants is nitrate and fluoride salt mixtures [23] [24] [25]. There is also some interest in concrete for lower-temperature storage [26]. However, the molten salts have several serious shortcomings. They have a relatively low range of temperatures where they are liquid, and they solidify at room temperature. Considerable engineering is required to keep them molten under all circumstances. Corrosion and chemical reactions from impurities cloud the long-term reliability picture.

The system proposed here uses sensible heat storage in solid graphite [24]. Nuclear reactors have used graphite as a moderator, heat exchanger and thermal store [27] HTGR. Thermal storage purity requirements for graphite are dramatically less than that for moderators, or even electrodes, which is a major use of graphite USGS. Graphite is quite cheap and abundant, especially mined graphite of 95%

purity. Our cost estimates use $2/kg, which is the cost of electrode graphite. Mined graphite is an abundant and cheaper alternative.

Graphite has good heat capacity, good thermal conductivity and maintains structural strength beyond 3000°C. Some issues are: graphite is porous and relatively weak and at high temperatures (above 800°C) it burns in the presence of oxygen. Nuclear reactor designs dealt with these issues. There, stacks of graphite blocks with channels for nuclear fuel and cooling fluid (high-pressure helium) were contained within a pressure vessel. The graphite had no structural requirement other than to support its own weight. Inert helium does not react with graphite and does not disassociate at high temperature. A constant pressure medium immersed the blocks, so the graphite experienced no pressure force. Incoming cold helium cooled the pressure vessel wall.

We propose to follow the nuclear reactor example, but instead of a large and difficult-to-manufacture pressure vessel, we propose to use many small pressure vessels. The reference design uses steel vessels 1 m in radius and 40 m long with a 2 cm wall thickness to build thermal accumulators. This is the domain of flat plate steel and conventional welding, so cost is low. The pressure of the helium coolant is 10 MPa. Graphite blocks with integral cooling channels are stacked within the accumulator. They are covered in a thermal insulating blanket, and there is a gap between the thermal insulator and the steel walls through which cold inlet and outlet helium flow. The cooling channels within the graphite blocks form a counter-flow heat exchanger, with one circuit transferring heat from the receiver to the graphite and the other circuit transferring heat from the graphite to the turbo generator. Both circuits operate independently allowing simultaneous thermal charge and discharge. A helium pump drives the circulating flow from the receiver. The compressor drives the flow in the circuit from the turbo generator. The steel walls are convection cooled externally in the event of a loss of pressurization or coolant. The thermal insulating blanket slows heat transfer to the steel walls.

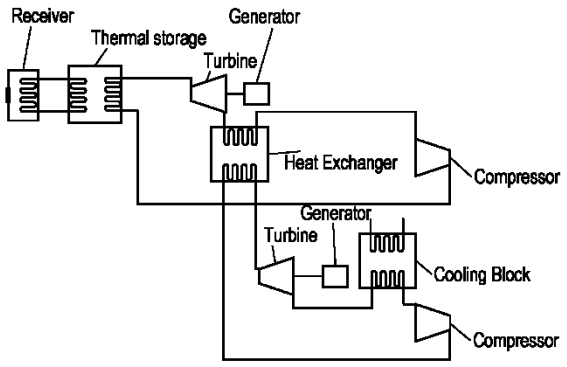

Figure 10

Figure 10 shows a schematic view of a thermal system with thermal storage as described above. In this case, we show a combined cycle system, which provides the best thermal efficiency and the best thermal storage efficiency. Light from the optical system arrives at the receiver on the left.

With sensible heat storage, the thermal energy stored depends on the temperature swing, the heat capacity and the density of the storage material. For an 800^{o} C temperature swing, graphite stores 0.2 kWh/kg thermal or 340 kWh/m^{3}. That is $10/kWh thermal at $2/kg graphite cost. Batteries cost at least $200/kWh electrical. Allowing for energy conversion efficiency, graphite thermal storage is about 10X cheaper than batteries. A higher temperature swing and/or cheaper graphite improve things even more. In addition, graphite does not have the reliability and useful life problems of batteries.

The 1 m radius, 40 m high thermal accumulator described earlier contains approximately 244,800 kg of graphite and stores 48,960 kWh. The accumulator wall contains 19,604 kg of steel. The cost of graphite clearly dominates the overall cost, particularly at $2/kg for graphite. The total cost of each 40-meter thermal accumulator is approximately $500,000. The steel enclosure and the graphite blocks can be shipped separately and the accumulators can be assembled on site. Storage capacity is modular in units of one accumulator, which accommodates a wide range of power plant sizes and options. This also facilitates standardization and large-scale production and distribution.

On the long-term technology roadmap, higher conversion efficiency comes from higher working gas temperatures. Sensible heat storage is synergistic with this trend because higher temperatures also lead to more storage capacity for the same amount of material. Graphite with helium working fluid used in the manner described above can easily scale in temperature, ultimately to 3000^{o} C plus. The limiting factor is the temperatures tolerated by interconnect piping and turbines. Given the need for an inert working fluid like helium, a logical material technology that would complement and enable this high-temperature technology roadmap is carbon-carbon composite [(28)].

Construction and operation:

The production manufacturing process for the mirror structure involves centrally manufacturing the structure, floating it up to 20km, and "flying" it to its destination. This is a delicate operation, much like deploying a deep-sea oil production platform, and requires similar attention to weather prediction. Buoyant “tugs” provide thrust. The construction of the “tugs” uses the same structural and buoyancy elements used to construct the mirror structures.

The tugs need the power of about 20 300kN thrust engines to propel the mirror, and have to plan every maneuver based on the wind. The tugs are the recovery mechanism for a mirror released in high wind.

The mirror structure operates in winds less than 25 m/s which occur more than 95% of the time. Above 25 m/s it switches to a “parked” horizontal low-drag configuration, just like ground-based heliostats. This reduces drag by more than a factor of ten. If a wind exceeds around 100m/s, an event not expected to occur during the lifetime of the power plant, we let the mirror loose, relieving the cantilever forces on the mirror structure. The tethered mirror has the ability to raise or lower to avoid wind. This should reduce the probability of freeing the mirror due to exposure to winds beyond 100 m/s.

Troposphere weather, particularly thunderstorms can push up into the low stratosphere, and there are various turbulence effects that NASA has well documented, again from troposphere effects pushing into the low stratosphere. Rising in altitude can avoid some of these effects.

The proposed light-pipe construction technique involves unwinding rolls of fabric and cable on the ground and assembling and joining them vertically as a buoyant top pulls the assembled wall up. Winding down the light-pipe allows for survival during extreme wind events. The extra step that allows winding down involves making the seams in a manner that allows opening and closing. A solution utilizing an industrial strength "Ziploc" for air tightness and mechanical fasteners for strength is necessary. At 1 m/s the light-pipe could be down in about 5 hours.

Winding down should be a rare event. The light pipe is resilient and when loosed from the mirror can blow over considerably without damage. A worst-case emergency backup mode could be to open sections of the fabric wall to reduce drag.

Hydrogen:

As discussed earlier, hydrogen gas provides the buoyancy required by the concentrator and the light-pipe. The use of hydrogen requires extensive engineering for fire protection and suppression. This engineering encompasses:

- Selecting non-flammable materials throughout
- Ensuring no buildup of static electricity
- Implementing lightning suppression
- Providing non-flammable buffer gasbags filled with nitrogen or argon to minimize hydrogen mixing with air in the case of a leak
- Ensuring adequate ventilation to avoid a hydrogen air buildup in any confined space
- Providing the equivalent of a "sprinkler system" using nitrogen gas or similar instead of water
- Providing emergency venting of gas bags
- Providing hydrogen-gas leak detectors, fire and smoke detectors

Ideally helium would be the gas of choice, but helium is expensive, and more importantly, a scarce resource [(29)]. The world supply of helium could not meet the demand of more than a few StratoSolar systems a year. Hydrogen is cheap, available in industrial quantities, and the supply can easily expand. Industry uses it extensively on a very large scale exceeding 50 million tonnes a year [(30)], and proponents of the hydrogen economy have done much to demonstrate its inherent safety characteristics [(31)].

Issues of concern:

There are significant challenges, as with any new large-scale engineering venture. Listed below are some concerns people have raised.

- The stratosphere is a harsh environment. UV, ozone, and cold are worse than at the ground

- Ice can form on the light-pipe. This could cause a falling-ice hazard or damage the light-pipe through excessive loading
- Wind damage could cause flying debris ripped from the light pipe or mirror
- The light-pipe or the mirror could fall down causing severe damage
- The systems might interact with the earth's atmospheric static charge, discharging it
- Lightning, static electricity
- Fire
- The optical surfaces, particularly the light-pipe wall may accumulate dust reducing optical efficiency by an excessive amount
- Planes can collide with the light-pipe, and possibly the mirror
- Terrorists or vandals could easily damage the light-pipe
- Wind forces on the light pipe will cause excessive motion through "galloping" resonance effects
- Wind forces are too large for the system to handle

Beyond electricity generation:

With a low-cost, high-quality thermal energy supply, other opportunities beyond electricity generation abound. These could be dedicated plants or more likely, hybrid plants. As was discussed earlier, the likely way to build electricity plants is to size the concentrator/receiver for winter sunlight. This means that there is a substantial excess seasonal supply of thermal energy. Many of the uses for process heat can adapt to this variable supply.

In addition, a permanent high altitude platform could serve many additional purposes. Listed below are some examples of process heat and communications uses.

- Process heat
  - Thermal desalination [32]
  - Thermal hydrogen, methanol, or gasoline generation [33] [30]
  - Metals furnace
  - Seasonal thermal storage

- Communications and observation platform
  - Cell phone tower, data networks
  - Radar for weather, commercial, military
  - Science
  - Laser communications network

With current, proven, large-scale multi-effect-distillation (MED), thermal desalination technology, plants that pump out a million m^3 of fresh water a day at \$0.25/m^3 are possible with StratoSolar providing the steam to drive the plant.

CSP cost compared to StratoSolar:

We have focused on the winter solstice DNSI because that is the number that should be used to size real solar plants. Yearly electricity demand does not follow the yearly supply of sunlight. A more constant electricity supply is required. Thermal storage enhances turbo generator utilization and allows for 24/7 electricity supply. Sizing the electricity turbo-generator using the energy available at the winter solstice, guarantees constant electricity output through the year. This means that, except near the winter solstice, some solar energy captured is discarded, or ideally is used for some other purpose (like desalination, district heating, hydrogen or methanol production, etc.). This also means the turbo generator has a high average utilization and the solar collector has lower average utilization.

As shown above, a solar collector at 20 km altitude gathers 3X more energy per m^2 than a ground-based CSP system. In addition, cosine losses for CSP heliostats at the ground give an aperture-to-mirror surface-area ratio of approximately 50%. A solar collector tracking the sun has at least 90% aperture-to-mirror surface-area ratio. This means that each m^2 of mirror at 20 km gathers approximately 5X to 6X more energy than each m^2 of ground-based CSP heliostat. An alternative perspective is StratoSolar needs one fifth to one sixth of the mirror area of CSP. Mirror surface area directly determines concentrator cost.

	Power Tower	StratoSolar
Insolation Winter (kWh/m^2/day)	5 to 6	12
Optical efficiency	45% to 50%	80% to 95%
Thermal efficiency	35% to 45 %	45% to 60%
Electrical (kWh/m^2/day)	0.8	4.8
Electrical (kWh/m^2/year)	287	1752
Mirror Assembly $/$m^2$	$150 to $300	$45 to $60
$/kW.h year	0.70	0.03
Cost for 8E9 kW.h	$5,566,427,484	$ 228,310,502

Table 5

Table 5 illustrates this calculation with representative numbers for current power tower CSP systems, such as the Brightsource Ivanpah facility, and StratoSolar [34].

The yearly electrical output of a 1GWe plant is 8e9 kWh. The input energy less the optical and thermal losses produce the daily and the yearly kWh/m^2. Dividing the $/$m^2$ by the kWh/m^2 results in the $/kWh which when multiplied by the yearly kWh yields the concentrator cost.

The $/$m^2$ cost can be better understood by considering it as the product of $/kg and kg/$m^2$. For glass and steel CSP heliostats, this is 30 to 60 kg/m^2 at about $5/kg. For StratoSolar this is 3 to 4 kg/m^2 at about $15/kg. The CSP structure is mostly heavy steel and glass and its material cost is low. The StratoSolar structure is mostly lightweight aluminum alloy, and its material cost is higher. These material costs represent fully fabricated-system costs, not raw-material costs.

This only compares the actual collector costs. Additional collector costs for ground-based CSP are the land cost and the construction cost to prepare the site and install the heliostat array. The land area required for a 1 GWe CSP system is about 120 km^2 assuming a flat site. This land and construction cost is an additional several billion dollars.

There is growing environmental concern concerning CSP plants. They have to keep the ground clean and clear of vegetation, which destroys the local habitat. They consume large volumes of water to regularly clean the mirrors, which is a big problem in the desert locations required for CSP. They also are far from population centers and existing transmission infrastructure, which requires expenditure of billions of dollars on new transmission lines. The Ivanpah facility is a good example of all these problems. The real cost of CSP plants rarely considers these additional costs.

StratoSolar power system financials:

Table 6

Capital Costs Breakdown ($)	**New Plant**	**Retrofit Plant**	**New Plant**	**Retrofit Plant**
Electrical Output (W)	**1,000,000,000**	**1,000,000,000**	**25,000,000**	**25,000,000**
Construction				
Earthwork	$ 42,857,143	$ 21,428,571	$ 1,071,429	$ 535,714
Concrete	$ 42,857,143	$ 21,428,571	$ 1,071,429	$ 535,714
Steel	$ 33,214,286	$ 16,607,143	$ 830,357	$ 415,179
Piping	$ 75,000,000	$ 37,500,000	$ 1,875,000	$ 937,500
Electrical	$ 110,714,286	$ 55,357,143	$ 2,767,857	$ 1,383,929
Instrumentation	$ 25,714,286	$ 12,857,143	$ 642,857	$ 321,429
Painting	$ 5,357,143	$ 2,678,571	$ 133,929	$ 66,964
Insulation	$ 17,857,143	$ 8,928,571	$ 446,429	$ 223,214
Building and Architectural	$ 24,285,714	$ 12,142,857	$ 607,143	$ 303,571
Construction Subtotal	$ 377,857,143	$ 188,928,571	$ 9,446,429	$ 4,723,214
Procurement		$ -	$ -	$ -
Power/Cooling Block	$ 400,000,000	$ -	$ 10,000,000	$ -
Thermal Storage	$ 300,000,000	$ -	$ 7,500,000	$ -
Receiver	$ 50,000,000	$ 50,000,000	$ 1,250,000	$ 1,250,000
Light Pipe	$ 120,000,000	$ 120,000,000	$ 50,000,000	$ 50,000,000
Mirror Assembly	$ 200,000,000	$ 200,000,000	$ 5,000,000	$ 4,000,000
Hydrogen	$ 31,500,000	$ 31,500,000	$ 8,400,000	$ 8,400,000
Development	$ 60,000,000	$ 60,000,000	$ 1,500,000	$ 1,500,000
Project Management	$ 40,000,000	$ 40,000,000	$ 1,000,000	$ 1,000,000
Engineering and Design	$ 20,000,000	$ 20,000,000	$ 500,000	$ 500,000
Start Up and Commissioning	$ 10,000,000	$ 10,000,000	$ 250,000	$ 250,000
Total Capitalized Cost ($)	**$ 1,609,357,143**	**$ 720,428,571**	**$ 94,846,429**	**$ 71,623,214**

Each power plant is a unique development. The costs shown in Table 6 are for California, and much of the data is from the California market price referent (MPR) spreadsheet. This is used to calculate the price for California power purchase agreements (PPA). The table covers four cases: a 1 GWe plant, a 1 GWe retrofit plant, a 25 MWe plant and a 25 MWe retrofit plant. Retrofit plants assume re-using the

site and equipment of a fossil fuel plant, and only adding a concentrator, light-pipe and receiver that pipes steam to the existing plant.

Power-plant construction is a long and complex process and involves many players shown as line items in Table 6.

- Development involves creating the project, raising the financing, getting regulatory approvals and picking the team of companies.
- Project management takes a design from the engineering and design contractor and manages construction and procurement of that design.
- Engineering and design produces the overall power plant design
- Construction involves the various areas listed.
- Procurement involves selecting and purchasing the large ticket items listed. Many of these involve some fabrication or assembly.

As can be seen, the solar elements comprise less than half the total capital cost for a utility scale plant.

Revenue and Income:

Table 7

	New Plant	**Retrofit Plant**	**New Plant**	**Retrofit Plant**
Electrical Output (W)	**1,000,000,000**	**1,000,000,000**	**25,000,000**	**25,000,000**
Utilization (%)	90%	45%	90%	45%
PPA Price ($/kW.h)	$ 0.12	$ 0.12	$ 0.12	$ 0.12
Total Revenue ($)	**$946,080,000**	**$473,040,000**	**$23,652,000**	**$11,826,000**
Insurance (high cost)	(16,343,571)	(9,343,571)	(1,004,714)	(766,232)
Property Taxes	($19,612,286)	($11,212,286)	($1,205,657)	($919,479)
Fixed O&M	($10,250,000)	($10,250,000)	($256,250)	($256,250)
Yearly Gross Profit	**$899,874,143**	**$442,234,143**	**$21,185,379**	**$9,884,039**
Interest	($138,920,357)	($79,420,357)	($8,540,071)	($6,512,973)
Depreciation(fed/state)	(61,288,393)	(35,038,393)	(3,767,679)	(2,873,371)
Amortized Annual Cost @8.5%	($144,447,762)	($82,580,358)	($8,879,866)	($6,772,113)
Taxes (state)	(61,850,421)	(28,975,345)	(784,782)	(43,996)
Taxes (Federal)	($223,235,240)	($104,580,017)	($2,832,496)	($158,795)
After Tax Cash Flow (first year)	$470,340,720	$226,098,423	$8,688,234	$2,909,135

Table 7 shows the revenue and expenses breakdown for the same four cases shown in Table 6.

Utilization is 90% for plants with thermal storage, and 45% for plants without thermal storage. The major factor affecting utilization is wind. Plants must "park" themselves when wind exceeds the operational design threshold.

The PPA negotiated prior to plant construction is a major determinant in financing. The current California PPA price is $0.12. The power plant size, utilization and the PPA set the revenue generated. Expenses include various taxes, insurance, fixed operation-and-maintenance (O&M) costs and the amortized annual cost of capital. The equity holders in the power plant receive the after-tax cash flow.

As can be seen, with the current level of PPA in California, StratoSolar plants are highly profitable. Even the pilot systems have profit potential.

Mirror structure manufacture and cost:

Table 8

		Production System	Pilot System
			1.94%
Strut length (m)		17.32	17.32
mirror diameter (m)		2300	**320**
surface area (m^2)		4,154,753	80,425
Struts/hexagonal panel		10	10
		159,926	3,096
struts for mirror side		**159,926**	**3,096**
struts for back side		**159,926**	**3,096**
Strut weight (kg)		10,704,744	207,215
Panels (kg)	at 1kg/m^2	4,154,753	80,425
Number of Hexagonal panels		**15,993**	**310**
Hexagonal Panel area		259.79	259.79
Hexagonal panel cost ($/m^2)		$ 12.00	$ 12.00
Panel cost ($)		**$ 3,117.51**	**$ 3,117.51**
Total cost all panels		$ 49,857,033	$ 965,096
Total cost of struts @$10/kg		$ 107,047,437	$ 2,072,147
number of struts/node		4.5	4.5
Total number of nodes		**71,078**	**1,376**
Node cost		$ 500	$ 500
Total cost of nodes		$ 35,539,087	$ 687,940
Hexagonal Panel depth (m)		1	1
Hexagonal wall area (m^2)		120	0
Wall weight (kg/m^2)		1	1
Hexagonal Mirror wall weight (kg)		120	0
panel kg/m^2		0.5	0.0
Circular panel wall area		54	54
Circular panel wall weight		54	54
Circular panel kg/m^2		0.2	0.2
kg lift /kg H		14	14
kg H		1,061,393	20,546
$H at $6/kg	6	$ 6,368,356	$ 123,274
Total kg/m^2		3.58	3.58
lift kg/m^3		0.1	0.1
m^3 /m^2		35.77	35.77
Total Cost		$ 192,443,557	$ 3,725,183
$/m^2		$ 46	$ 46
kg/m^2		3.6	3.6
$/kg		$ 12.95	$ 12.95

Table 8 shows a bottom-up cost analysis for a variety of mirror structures based on a tetrahedral truss design. It itemizes the individual components, their individual costs, and their total numbers and total cost. The components are triangular aluminum struts, nodes, which include node electronics, hexagonal

mirror segments and hydrogen gas. The right-hand column covers the pilot system and the second from the right covers a production system. The bottom line reduces the cost to a $/kg number for comparison with the top-down analysis.

The top-down analysis simply takes the total mass in kg and uses an estimate of $/kg based on experience to estimate total cost. The construction and shipbuilding industries use this method for preliminary cost analysis and as a crosscheck against bottom-up cost analysis. These two industries are similar in style to StratoSolar.

For example, cargo ships, which are complex items with many subsystems, can be reasonably cost estimated from a material cost per kg for flat plate steel (about $0.7/kg) with a multiple of two for labor cost. This results in about $1.5/kg for ships [(35)].

Aluminum alloy costs about $2/kg. If we estimate fabrication and assembly as a 7.5X multiple of material cost, we get a cost of $15/kg for the mirror structure. The bottom up analysis is $12.96/kg, a little lower.

A high productivity centralized factory utilizing mass produced standard elements will manufacture the mirror structure, making the cost estimates reasonably conservative.

Light pipe cost analysis:

The light-pipe is predominantly a thin wall, and a top-down cost estimate is best represented as $/$m^2$. The surface area is around 6 million m^2 for a 50 m radius light-pipe, and 1.8 million m^2 for a 15 m radius light pipe. For a steel-cable reinforced wall, we estimate $35/$m^2$, and for Kevlar, we estimate $40/$m^2$ based on the quantities of material calculated in wind-load simulations. The dominant cost is the material required for strength.

The light-pipe surface fabric and reinforcing cables are unrolled from winches. The fabric seams will be "zippered together" as the pipe grows. This is effectively like a current tethered-blimp deployment, but using multiple tethers that join to make a single hollow tether. For maintenance, in emergencies, or if extreme weather events are forecast, the light-pipe is lowered by the same mechanism. At 1 m/s, it takes about 5 hours to raise or lower the light-pipe.

Cost of StratoSolar with increasing latitude:

One of the biggest benefits of the StratoSolar approach is the flexibility in locating power plants, and in particular the ability to realistically build systems as far north or south as latitude 60 degrees. There are tradeoffs and costs for 24/7 systems. Table 9 shows some tradeoffs for different latitudes and different generation utilizations.

Table 9

Latitude	Daylight Hours	Mirror Area (km^2)	Mirror Radius	Thermal Storage (kW.hr)	Cost $B	Electricity kWh/Year	LEC 10% ($/kWh)	LEC 5% ($/kWh)
	Constant 1GWe							
59	6	8.333	1,629	36,000,000	$ 1.62	8.0E+09	$ 0.028	$0.013
55	7	7.143	1,508	34,000,000	$ 1.51	8.0E+09	$ 0.027	$0.012
50	8	6.250	1,410	32,000,000	$ 1.42	8.0E+09	$ 0.025	$0.011
42	9	5.556	1,330	30,000,000	$ 1.33	8.0E+09	$ 0.024	$0.010
31	10	5.000	1,262	28,000,000	$ 1.26	8.0E+09	$ 0.022	$0.010
	12 hour 1GWe , 12 hour .5GWe							
59	6	6.250	1,410	24,000,000	$ 1.26	6.0E+09	$ 0.030	$0.013
55	7	5.357	1,306	22,000,000	$ 1.16	6.0E+09	$ 0.028	$0.012
50	8	4.688	1,222	20,000,000	$ 1.08	6.0E+09	$ 0.026	$0.012
42	9	4.167	1,152	18,000,000	$ 1.01	6.0E+09	$ 0.024	$0.011
31	10	3.750	1,093	16,000,000	$ 0.95	6.0E+09	$ 0.022	$0.010
	1GWe daytime only, seasonal variation, no storage							
59	6	2.083	814	-	$ 0.53	4.0E+09	$ 0.019	$0.009
55	7	2.083	814	-	$ 0.53	4.0E+09	$ 0.019	$0.009
50	8	2.083	814	-	$ 0.53	4.0E+09	$ 0.019	$0.009
42	9	2.083	814	-	$ 0.53	4.0E+09	$ 0.019	$0.009
31	10	2.083	814	-	$ 0.53	4.0E+09	$ 0.019	$0.009

Three different scenarios for 1 GWe generation are covered. The first (on the bottom) is 1 GWe with no thermal storage. This produces the smallest amount of electricity (4e9 kWh/year) at the lowest capital and operational cost but with a large seasonal variation. The seasonal variation grows larger with higher latitude. Note that all latitudes produce the same total kWh/year. As can be seen the levelized electricity cost (LEC) depends heavily on the working average cost of capital (WACC).

The second scenario (in the middle) assumes thermal storage that provides for a constant 1 GWe for 12 hours and .5 GWe for 12 hours, providing 6e9 kWh/year. This matches the average electricity demand curve. As can be seen, more thermal storage and larger solar collectors are needed as latitude grows, raising the LEC. However, the increase is from a low of $0.01/kWh to a high of $0.013/kWh at a WACC of 5%.

The third case (on top) is 1 GWe for 24/7. This also shows increased cost with higher latitude, but the LEC is hardly changed. This is because more kWh of electricity supply balances the higher capital cost for more thermal storage and bigger mirrors.

List of abbreviations:

DNSI	Direct Normal Solar Insolation
CSP	Concentrated Solar Power
CPC	Compound Parabolic Concentrator
kWh	kilo Watt hours
GWe	Giga Watt electrical
Pa	Pascals
MPa	Mega Pascals
PPA	Power Purchase Agreement
ppm	part per million
PET	polyethylene terephthalate
mrad	milli radian
LEC	Levelized Electricity Cost
O&M	Operation and Maintenance
R&D	Research and Development
WACC	Working Average Cost of Capital
OLF	Optical Light Film
Wh	Watt hours
HAA	High Altitude Airship
UV	Ultra Violet
UHMWPE	Ultra-high-molecular-weight polyethylene

Bibliography

1. TCOM home page. *TCOM.* [Online] 2010. http://www.tcomlp.com/aerostats.html.

2. *POST: A stratospheric telescope for the Antartic.* **Michael A. Dopita, Holland C. Ford, John Bally, Pierre Bely.** 13, s.l. : Astron. Soc. Aust., 1996, Astron. Soc. Aust., pp. 48-59.

3. **Gregory J. Kolb et al.** *Heliostat Cost Reduction Study.* Albuquerque, NM : Sandia National Laboratories, 2007.

4. **L. M. Murphy, J. V. Anderson, W. Short, T. Wendelin.** *System performance and cost sensitivity comparisons of stretched membrane heliostat reflectors with current generation glass/metal concepts.* Golden, CO : SERI, 1985.

5. **Gary Jorgensen et al.** *Advanced reflector materials for solar concentrators.* Golden, Co : NREL, 1995.

6. **A. Palisoc, G. Veal, C. Cassapakis, G. Greschik, M. Mikulas.** *Geometry attained by pressurized membranes.* Tustin, CA : L'Garde, Inc.,, 1998.

7. **Frederick H. Redell, Justin Kleber, David Lichodziejewski, Dr. Gyula Greschik.** *Inflatable-Rigidizable Solar Concentrators for Space Power Applications.* Tustin, CA : L'Garde Inc.,, 2004.

8. **E. Onate, B. Kroplin.** *Textile composites and inflatable structures II.* s.l. : Springer, 2008. ISBN 978-1-4020-6855-3.

9. **Roland Winston, Juan C. Minano, Pablo Benitez.** *Nonimigaing Optics.* s.l. : Elseveir, 2005. ISBN-13:978-0-12-759751-5.

10. **Imke Durre, Russell S. Vose, David B. Wuertz.** *Overview of the Integrated Global Radiosonde Archive.* Asheville, NC : National Cimatic Data Center, 2006.

11. *Enhanced radiosonde data for studies of vertical structure.* **Imke Durre, Xungang Yin.** 2008, BAMS, pp. 1257-1262.

12. **George D. Modica, Thomas Nehrkom, Thomas Myers.** *An investigation of stratospheric winds in support of the high altitude airship.* Lexington, MA : Atmospheric and environmental research Inc., 2006.

13. *Air mass and refraction.* **Young, A. T.** s.l. : Applied Optics. 33:1108–1110, 1991, Vol. 33, pp. 1108–1110.

14. **Tiwari, G.N.** *Solar energy.* s.l. : Alpha science international inc., 2002. ISBN 978-1-84265-106-3.

15. **John A. Duffie, William A. Beckman.** *Solar Engineering of thermal processes.* s.l. : John Wiley and sons, Inc.,, 2006. ISBN-13 978-0-471-69867-8.

16. **Holms, John D.** *Wind loading of structures.* s.l. : Taylor and Francis, 2001. ISBN10: 0-415-40946-2.

17. **Whitehead, Lorne A.** *Prism Light Guide having surfaces which are in octature. 4,260,220* USA, 1981.

18. **Steven G. Saxe, Lorne A. Whitehead, Sanford Cobb, Jr.** *Progress in the development of prism light guides.* St Paul, Mn : 3M Optics technology Center, 1985.

19. *Evaluation of diffraction loss in prism light guides by finite-difference time-domain field modeling.* **Whitehead, Lorne A.** 1998, Applied Optics, p. 5836 to 5842.

20. *Parameterized transmittance model for direct beam and circumsolar spectral irradiance.* **Gueymard, Christian A.** 2001, Solar energy, pp. 325, 346.

21. **Ursula Murschall, Ulrich kern, Andreas Stopp, Guenther Crass.** *Transparent, UV resistant,thermoformable film made from crystallizable thermoplastics, and process for its production. 6,902,818 B2* USA, 2005.

22. *Helium turbomachine design for GT-MHR plant.* **C. F. McDonald, R. J. Orlando, G. M. Cotzas.** Phoenix, AZ : ASME, 1994. International Joint Power generation conference.

23. **James E. Pacheco, Hugh E. Reilly, Gregory J. Colb, Craig E. Tyner.** *Summary of the solar two test and evaluation program.* Albuquerque, NM : Sandia National laboratories, 2000.

24. *High-Temperature Liquid-Fluoride-salt closed-Brayton-cycle solar power towers.* **Charls W. Forsberg, Per F. Peterson, Haihua Zhao.** s.l. : Journal of solar energy engineering, 2007, Vol. 129, pp. 141-146.

25. **Litwin, Robert Z., Hoffman, Nathan J., Zillmer, Andrew J.** *High temperature molten salt solar receiver. 479635* 2006.

26. *Concrete storage for solar thermal power plants and industrial process heat.* **Doerte Laing, Dorothea Lehmann, Carstan Bahl.** 2008. International renewable energy storage conference.

27. **M. P. LaBar, A. S. Shenoy, W. A. Simon, E. M. Campbell.** *The gas-turbine modular helium reactor.* San Diego, CA : General Atomics, 2000.

28. **Per F. Peterson, Charles W. Forsberg, Paul S. Pickard.** *Advanced CSiC composites for high-temperature nuclear heat transport with helium, molten salts, and sulfu-iodine thermochemicalhydrogen process fluids.* s.l. : Argonne National Laboratory, 2002.

29. **D. M. Smith, W. Goodwin, J. A. Schillinger.** *Challanges to the worldwide supply of helium in the next decade.* Allentown, PA : Air Products and Chemicals Inc., 2002.

30. **George A. Olah, Alain Goeppert, G. K. Prakash.** *Beyond oil and gas: the methanol economy.* s.l. : Wiley-VCH, 2006. ISBN-13: 978-3-527-31275-7.

31. **Lovins, Amory B.** *20 Hydrogen myths.* s.l. : Rocky Mountain Institute, 2005.

32. *Desalination: present and future.* **Semiat, Raphael.** s.l. : Water International, 2000, Vol. 25, pp. 54-65.

33. *Thermochemical solar hydrogen generation.* **Licht, Stuart.** s.l. : The royal society of chemistry, 2005, pp. 4635-4646.

34. **Greg Kolb et al.** *Heliostat cost reduction.* s.l. : Sandia National Laboratories, 2007.

35. **Jonathan M. Ross.** *A Practical Approach for Ship Construction Cost Estimating.* s.l. : Proteus Engineering, Anteon Corporation, U.S.A., jross@anteon.com, 2004.

Appendix

Prototype system drawings, Google Earth views and informative pictures

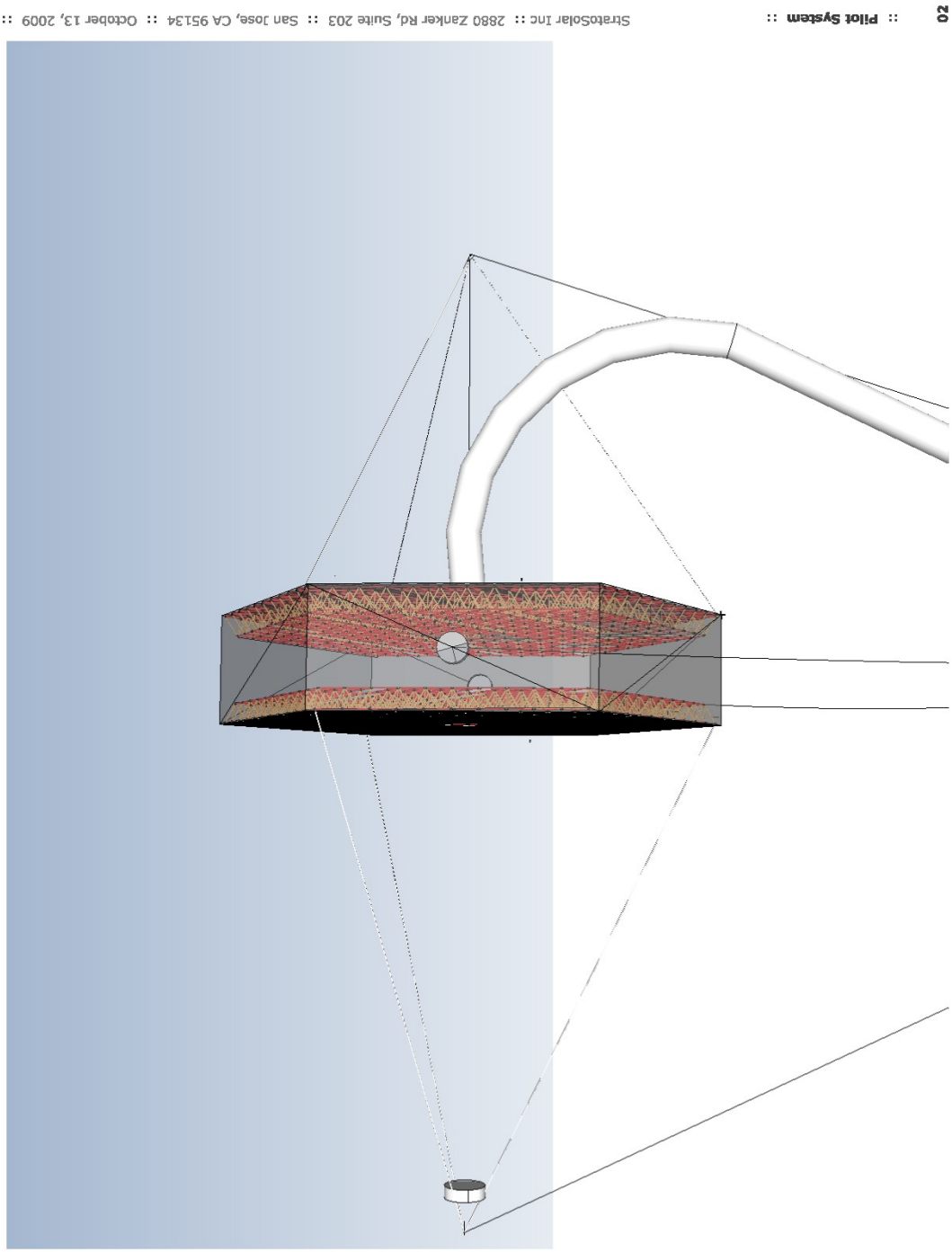

Figure 11

These drawings show elements of a prototype 25 MWe system. Figure 11 and Figure 12 show a side view of a prototype-system mirror-assembly. These drawings are only partially complete and serve to illustrate some possible design choices. Firstly, the optical system is a symmetrical Cassegrain. The secondary reflector is a convex, hyperbolic surface. This configuration requires a "hole" in the mirror

center. The light pipe entry is at the back of the mirror, and the light pipe has to curve awkwardly to connect to the tether.

The front and rear surfaces are constructed from a tetrahedral truss. The inner truss elements are not shown. The surfaces are shown as flat, which implies a Fresnel-like optics. It is also straightforward to curve the truss structure to a paraboloid.

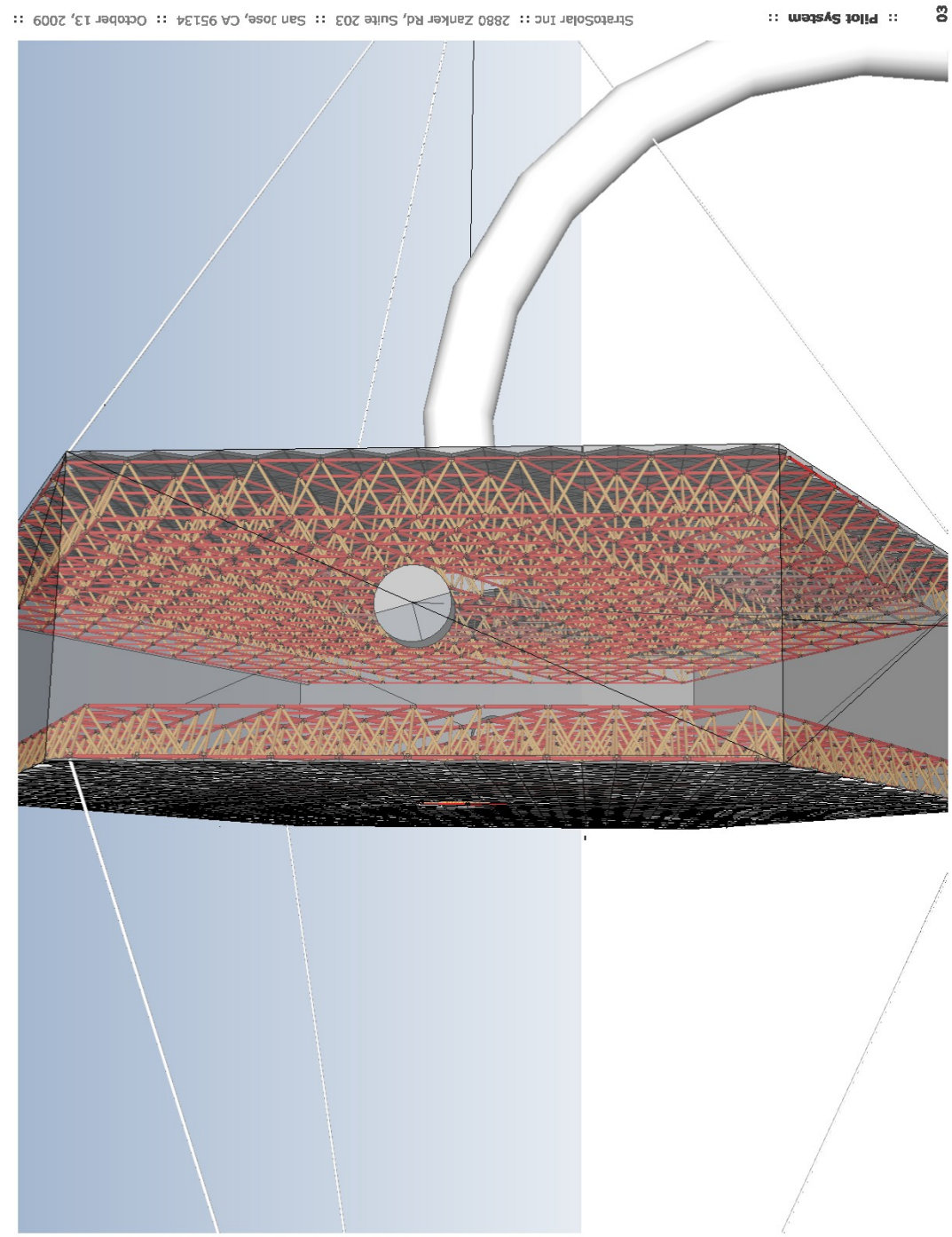
:: October 13, 2009 :: San Jose, CA 95134 :: 2880 Zanker Rd, Suite 203 :: StratoSolar Inc ::
:: Pilot System ::
03

Figure 12

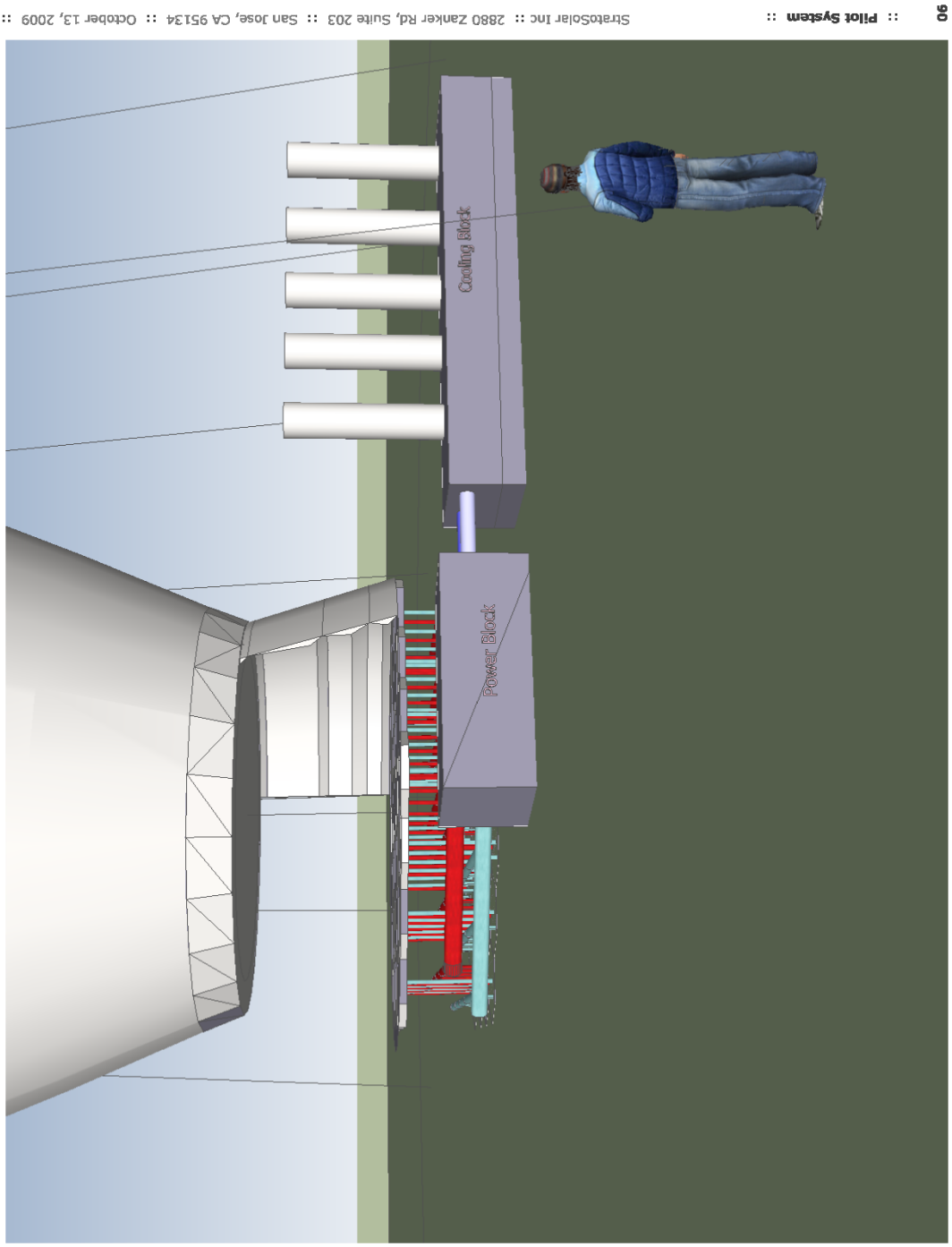

Figure 13

Figure 13 shows a ground level view of the prototype 25 MWe receiver, power block and cooling block. The figure also shows the bottom of the CPC and a portion of a cavity wall.

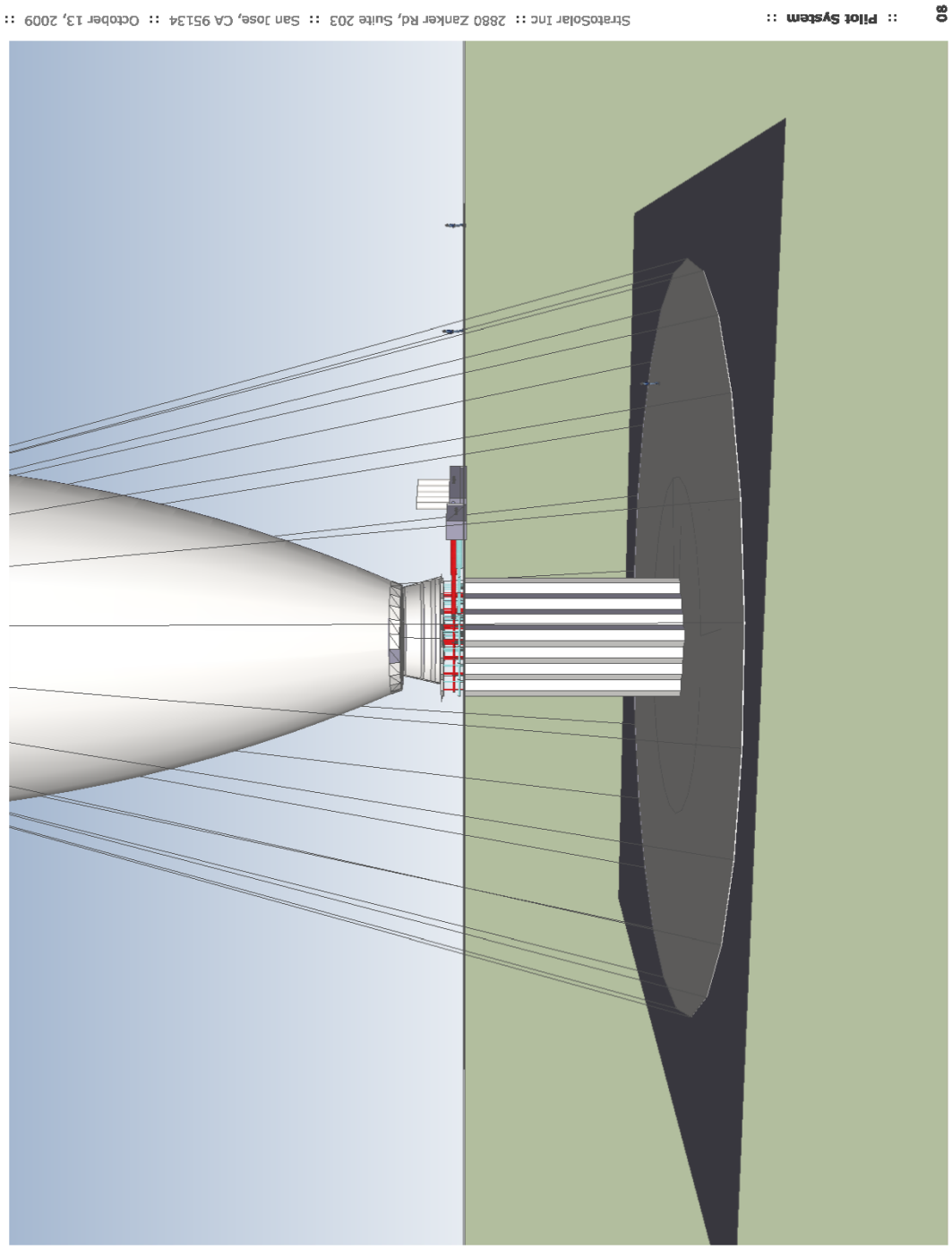

Figure 14

Figure 14 shows the below ground thermal storage elements.

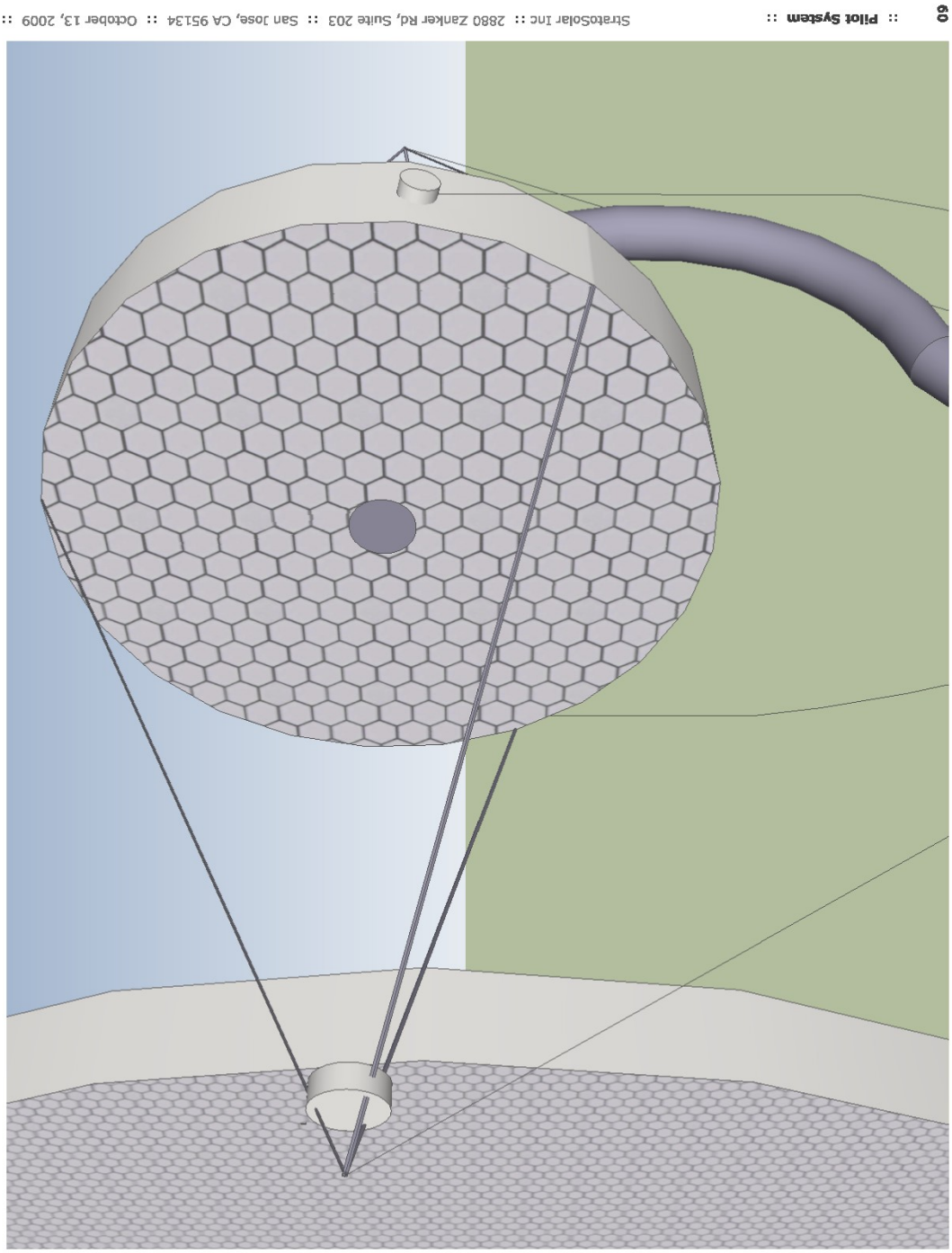

Figure 15

Figure 15 shows a simplified mirror for a 25 MWe mirror with appropriately sized hexagonal mirror-segments. For comparison, a portion of a full size 1 GWe system mirror using the same mirror-segments is also visible.

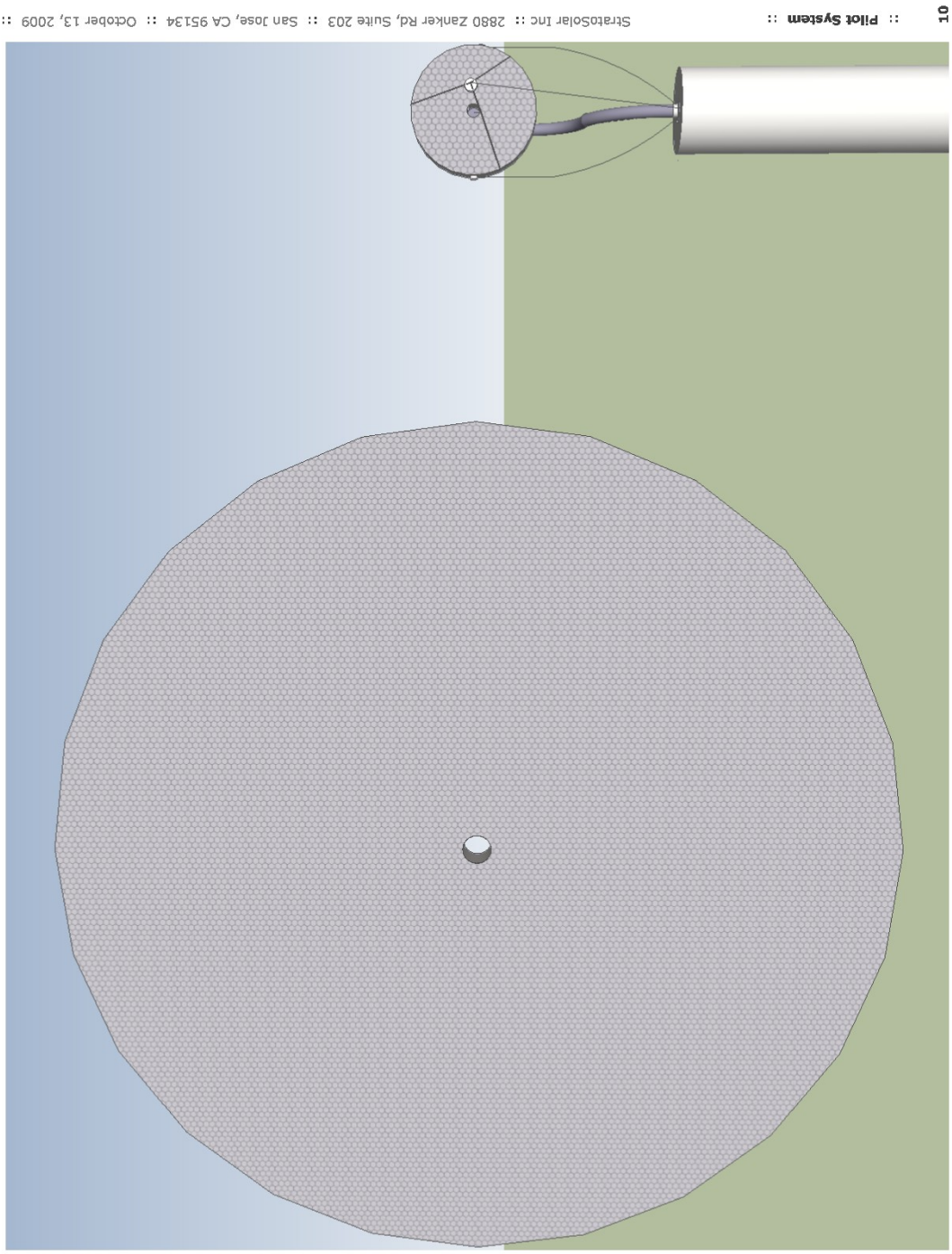

Figure 16

Figure 16 shows the relative size of a 25 MWe mirror and a 1 GWe mirror. The top of the buoyancy sleeve for the 25 MWe system is also visible.

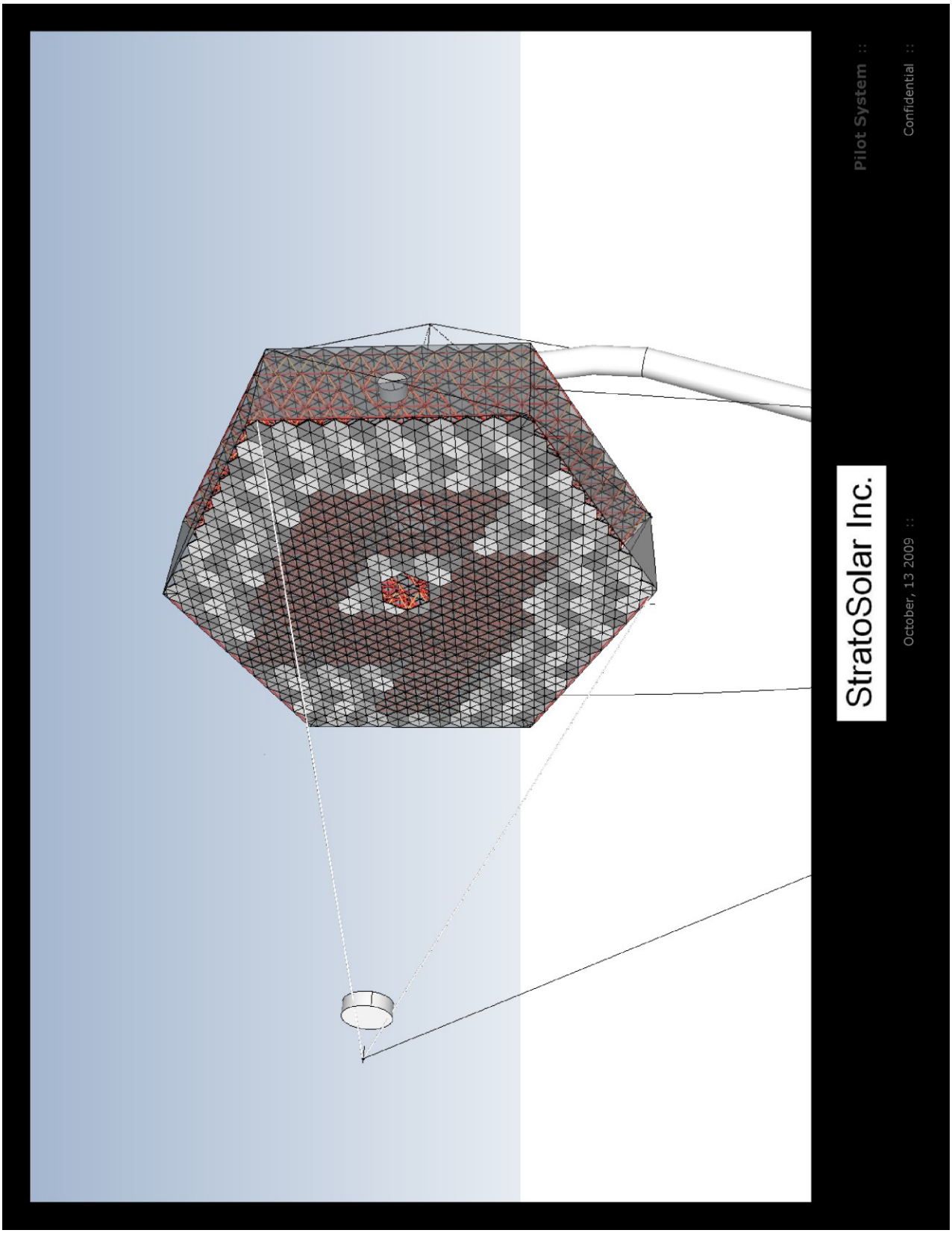
Pilot System ::
Confidential ::
StratoSolar Inc.
October, 13 2009 ::

Figure 17

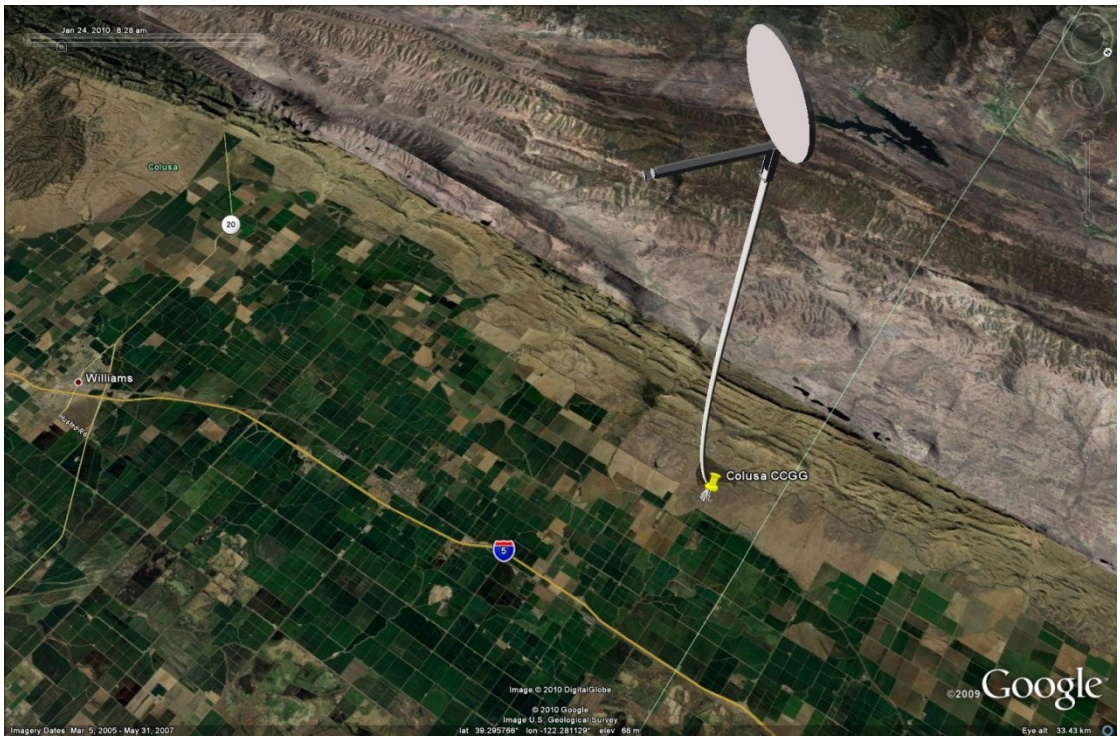

Figure 18 **Colusa at dawn on winter solstice from above**

Figure 19 **Colusa at dawn on winter solstice from I5**

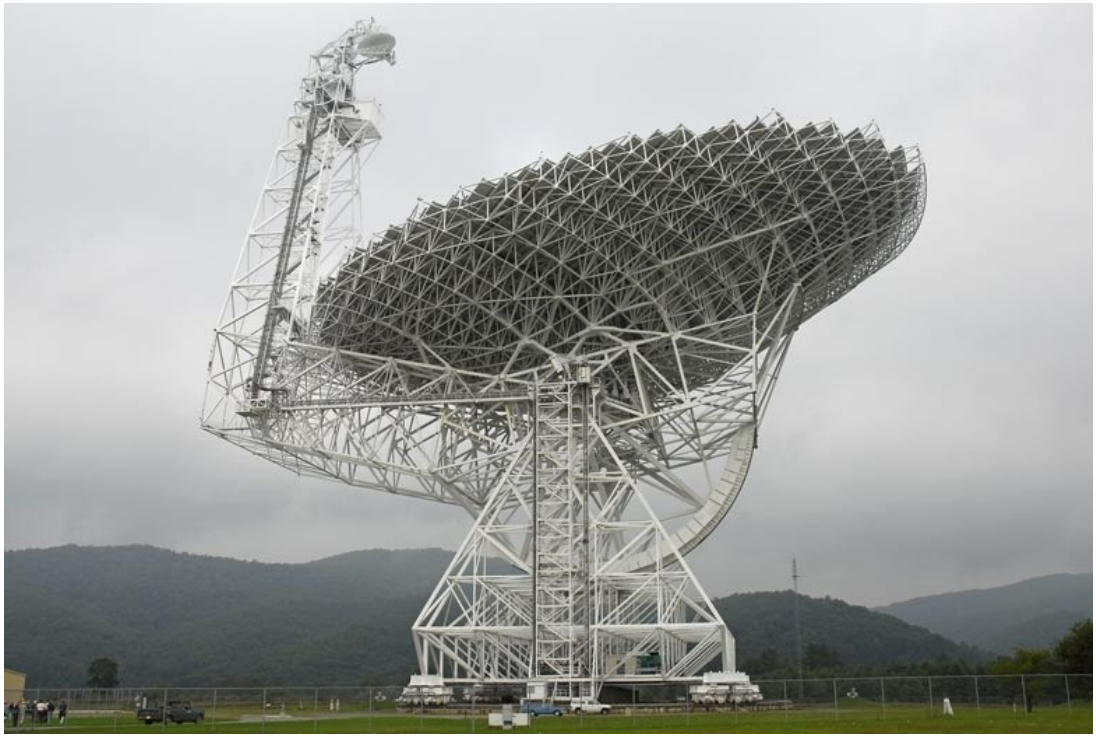

Figure 20 Green Bank radio telescope

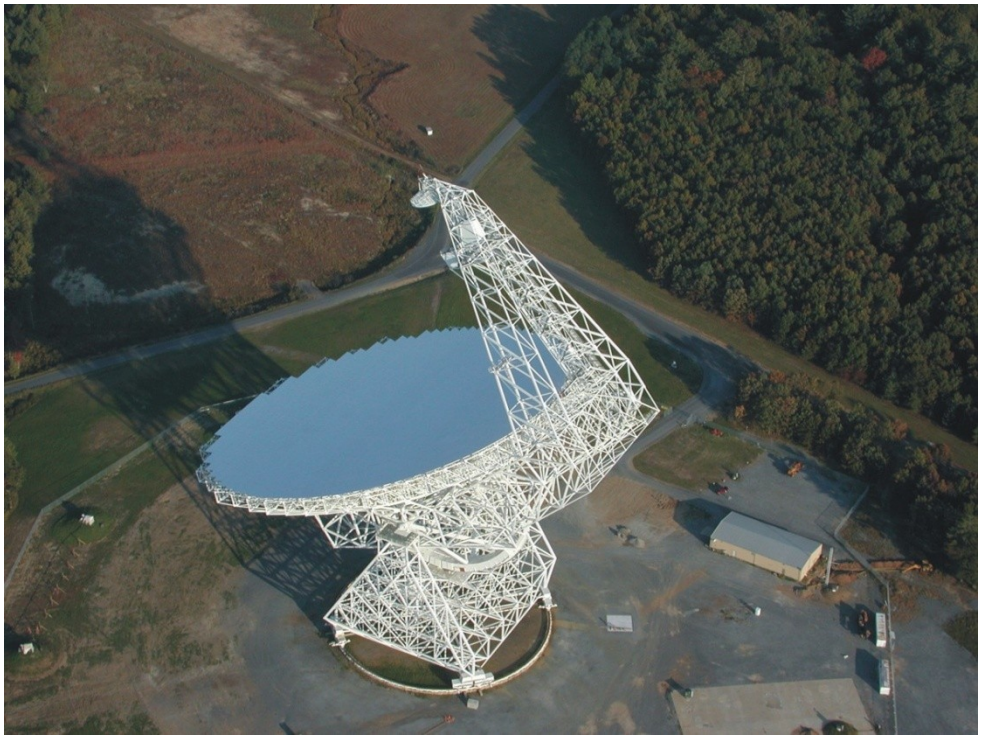

Figure 21 Green Bank radio telescope

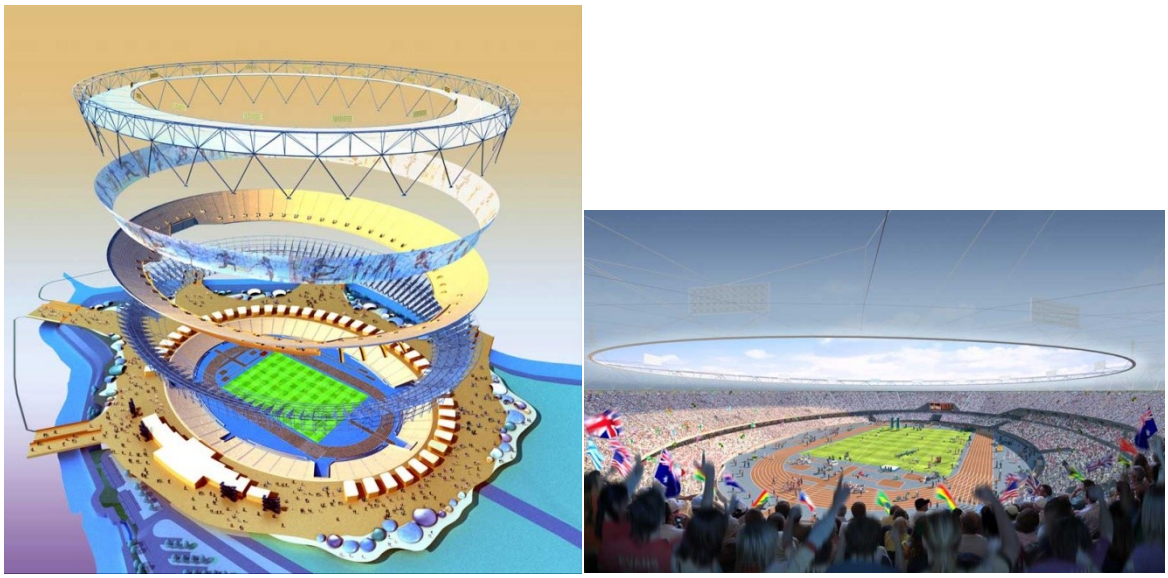

Figure 22 London Olympic stadium fabric roof

Figure 23 Vancouver dome

Figure 24 Berlin Olympic stadium

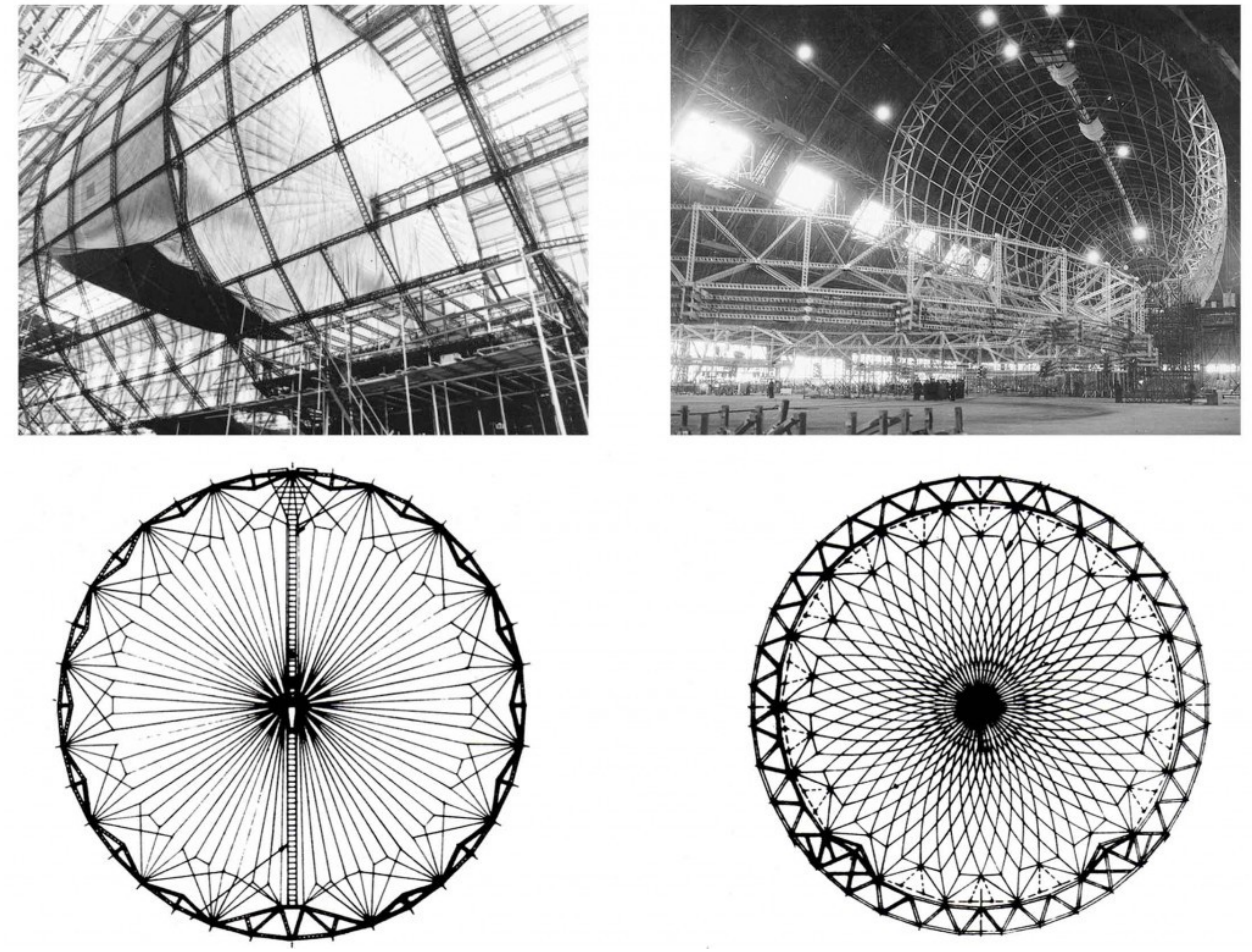

Figure 25 Internal structure of the Hindenburg and the Macon

Figure 26 Air force tethered aerostat radar